DOT/FAA/CT-03-91-C-00044
FAA Technical Center
Atlantic City Airport
N.J. 08405

Development of an Improved Biodynamic Model for SOM-LA/TA

Dr. Hamid M. Lankarani
Shashishekar Shivaswamy

National Institute for Aviation Research
Wichita State University
Wichita, KS 67260-0093

September 1994

Final Report

DEVELOPMENT OF AN IMPROVED BIODYNAMICS MODEL FOR SOM-LA/TA

Final Report DOT/FAA/CT-03-91-C-00044

Principal Investigator: Hamid M. Lankarani
National Institute for Aviation Research
Wichita State University
Wichita, KS 67226-0035

ABSTRACT

An improvised SOM-LA/TA biodynamics model has been developed for the Hybrid II Anthropomorphic Test Dummy (ATD). This improved model more accurately predicts the HIC and lumbar load of an ATD subjected to the dynamic tests specified in FAR Part 23.562.b(1) & (2). Then dynamic tests were conducted at the Impact Dynamics Laboratory at National Institute for Aviation Research at various deceleration loads of 14, 19, 25 and 32 g's. The effect of the occupant size on the response os a seat/ occupant/ restraint system was studied by the construction of a few non-standard occupant data bases. In an effort to improve the head injury protection for passengers seated behind interior walls in transport aircraft, a head strike test apparatus was designed and constructed. Preliminary tests were conducted to evaluate Head Injury criteria (HIC)using the head component tests. Suitable energy absorbing padding materials were identified using both analytical and experimental measures. Guidelines were also developed for design and development of infant and child seats and restraint systems.

Finally, recommendations for further improvements and research to be carried out is discussed.

TABLE OF CONTENTS

TABLE OF CONTENTS (Cont)

LIST OF ILLUSTRATIONS

LIST OF ILLUSTRATIONS (Cont)

LIST OF ILLUSTRATIONS (Cont)

LIST OF ILLUSTRATIONS (Cont)

LIST OF TABLES

EXECUTIVE SUMMARY

Federal Aviation Regulations (FAR's) pertain to the performance (response) of the seat structure, the restraint system and the occupant. Analytical capabilities are needed to predict the occupant response in different aircraft crash configurations. Existing occupant models, including SOM-LA/TA (Seat Occupant Model - Light Aircraft/ Transport Aircraft) have deficiencies in accurate prediction of such measures as lumbar loads.

In this project, dynamic tests were conducted using Hybrid II ATD seated on an iron seat, which is representative of typical commuter aircraft geometry. The tests were conducted at the Impact Dynamics Laboratory at National Institute for Aviation Research. The Kodak Ektapro system was employed to quantify the position, velocity and accelerations of the imaging target affixed to some points on the ATD and the seat frame. These tests were conducted as per FAR part 23.562.b(1) & (2) at various decelleration levels (14, 19, 25 & 32 g's). Several of the pulses used in these tests correspond to those specified in the FAR's. The 25 g test was proposed to provide for evenly spaced data points. A two-point restraint system was employed in this test series.

The SOM-LA/TA occupant model was modified to improve the accuracy of the predicted occupant response for position, velocity and acceleration of occupant segments, loads and injury measures. These modifications included the development of a nonlinear finite element model of the ATD lumbar spine for better prediction of the lumbar load and development of occupant envelope for secondary impact of the ATD onto the surroundings. Analysis of the seat structure was also conducted using the concept of plastic hinges and compared to the nonlinear FE model of a general aviation seat. The dynamic tests conducted earlier were then simulated using the original SOM-LA/TA code, MADYMO and ATB. All the codes showed reasonable degree of accuracy, except the modified SOM-LA/TA providing much closer results in the lumber load.

Designed and fabricated a Head Strike Test (HST) apparatus . Specific design was selected from feasibility studies reported earlier. The approach permits impact tests of a HYBRID II ATD head only against various materials, simulating typical seat backs/ bulkheads. Preliminary tests were conducted on the apparatus and the HIC were evaluated to obtain parametric information concerning various materials impacted to facilitate selection of appropriate materials for the bulkhead and inter walls by designers.

SOM-LA/TA models were identified which were representative of occupant other than the 50% male. The effort was concentrated on a 3 year old child data. In addition all the injury criteria were assessed and the method of scaling was used to determine the injury criteria for

occupants, guidelines
ıs. A beginning study
ɔy analytic means.

NO REF
TO FAA
SPON SORS

1. DYNAMIC TESTING AND SIMULATION OF OCCUPANT RESPONSE

1.1 Introduction

Dynamic testing of anthromorphic test dummies (ATD) is crucial for the evaluation of the survivability of occupant during an aircraft crash. Lumbar load and the Head Injury Criteria (HIC) indicate are among means for amount of the occupant injuries. An adult represented by Hybrid II dummy, is said to have received fatal injuries when the value of lumbar load exceeds 1500 lb or when the value of HIC exceeds 1000. Many factors like the seat structure, seat cushion and restraint system affect the response of the occupant.

In this project, a series of dynamic sled tests were conducted at the Impact Dynamics Lab at NIAR. Tests were conducted on 50 th percentile Hybrid II dummy on an iron seat according to FAR Part 23.562.b(1) & b(2) deceleration pulses. Computer codes including SOM-LA/TA, MADYMO and ATB were used for simulating the crash and their performances were evaluated by comparing the results with the actual test results [1, 2]. Sample of the results are presented in this section.

1.2 Occupant response at 19G deceleration pulse with seat at 60^0 pitch

Dynamic test was conducted to analyze the occupant response to 19G deceleration pulse as specified by the FAR for commuter aircraft. A 50th percentile Hybrid II dummy was used as the occupant and the seat used was an almost rigid (iron) seat, which is representative of a typical commuter aircraft geometry. The test conducted had a peak deceleration of 19G and a duration of 100 milliseconds. The test was conducted according to FAR part 23.562.b(1) specification. The ATD was restrained by a lap belt and the seat was inclined at 60 degree to the horizontal. The test was also simulated using the software SOM-LA/TA, MADYMO and ATB available at the NIAR/WSU. Head resultant acceleration, HIC and lumbar load were compared to determine the validity of the software. Figure 1.1 represents the plot of the resultant head acceleration and Figure 1.2 represents the plot of lumbar load. Table 1.1 represents the HIC values and the peak values of lumbar load. Lumbar load values were not obtained from ATB, since ATB does not have provision to analysis the lumbar load. From Figure (1.1), it is clear that, the peak values from these analysis codes and the test results are almost similar for the head acceleration curves [1], but the trends are quite different. The lumbar load obtained from MADYMO is much closer to the experimental values than the values obtained from SOM-LA/TA.

1.3 Occupant response at 26G deceleration pulse with seat at 60^0 pitch

Dynamic sled test at 26G deceleration pulse as per FAR Part 23.562.b(1) was conducted in order to better evaluate the proposed regulations for commuter aircraft category. A 50th percentile Hybrid II ATD was used as the occupant with a lap belt and the seat used was a rigid (iron) seat, which is representative of a typical commuter aircraft seat. The seat was inclined at 60 degree to the horizontal as per FAR Part 23.562.b(1). The tests were then simulated on the computer codes SOM-LA/TA, MADYMO, and ATB. Head resultant acceleration, HIC and

Lumbar load obtained from the computer simulation were then compared with the sled test result [1]. Figures 1.3 and 1.4 represent the resultant head acceleration and lumbar load respectively. Table 2.2 gives the peak values of lumbar load and HIC for this test. From Figures 1.3 and 1.4 it is clear that at higher deceleration levels the computer codes are less efficient in predicting the sled test results. Same trend was observed for the lumbar load too. The head acceleration and HIC value predicted by MADYMO are higher than the test results. Good HIC correlation was obtained from ATB.

1.4 Occupant response at 15G deceleration with seat at 10^0 yaw

Dynamic sled test with the seat inclined at 10 degree yaw to the vertical as per FAR 23.562.b(2) conditions, was conducted. As a first step, sled experiment was performed for a triangular deceleration pulse of 15G. A 50th percentile Hybrid II dummy was used as the occupant. Initially a lap belt was used as the restraint. However this resulted in the impact of the dummy head with the dummy knees. Therefore the restraint system was changed to a 4 point restraint system. The seat used was again a rigid (iron) seat. The tests were then simulated on the computer codes SOM-LA/TA, MADYMO, and ATB. The 3 dimensional occupant models were used in the simulations. Head resultant acceleration and HIC then compared with the test results [1]. Figure 1.5 represents the resultant head acceleration of Hybrid II dummy subjected to a triangular 15G pulse with the seat at 10 degree yaw . Table 2.3 gives HIC value of the test and from the simulations.

The difference in the simulation results can be attributed to various sources. For example, the model parameters like segment weight distribution, damping and stiffness coefficient of joints and the articulation of body segments play a major role in these differences. The 3-dimensional occupant model of SOM-LA/TA has 12 segments, while MADYMO and ATB have 13 and 15 segments respectively. Also the spinal column of SOM-LA/TA is modelled without any weight. One of the most important parameter that affects the results is the contact points of the restraint systems with the occupant segments. All the software assume the occupant segments to be made up of ellipsoids. The restraint systems are specified such that they are tangent to these ellipsoids. The difference in their dimensions will change the point of contact of the restraint system with the occupant body, which in turn results in output that are different from other models. The other parameters that affects the results are differences in body segment masses, moment of inertia, mass center of body segments, body contact surface radius, flexion and extension angles of body segments and the type of joints that connect the body segments. Apart from these parameters, the elastic properties such as, flexural and torsional stiffness, flexural and torsional damping, friction coefficients between the body segments and the contact parameters between the occupant and seat or floor will also influence the results.

1.5 Occupant response at 19G deceleration with seat at 10^0 yaw

Simulation of sled impact test at 19G deceleration pulse with the seat at 10 yaw to the vertical was carried out using the developed occupant modeling and analysis capabilities and also other codes such as Madymo and ATB. The tests were carried out for Hybrid II dummy for

19G acceleration pulse with the seat at 10^0 yaw. The results are shown in Figure 1.6. It can be seen the computer simulation only predicts the peak values of head acceleration reasonably well. However, the existing variation shows that the analysis software still have some difficulties in 3-D modeling of the occupant.

1.6 Remarks

The simulation results were in reasonable agreement with the experimental results for the position and velocities at low deceleration levels for peak magnitudes of acceleration. At high deceleration levels, the results were not totally reliable. The performance of the codes can be improved by modelling the elements as flexible instead of being rigid. Improvements in the performance of code SOM-LA/TA was noticed when the spine was modelled as a flexible member. This is described in detail in the next chapter.

1.7 References

1.Lankarani, H.M., "Teat Program: A94026, 14CFR 23.562," Impact Dynamics Laboratory, NIAR, The Wichita State University, Jan 1994.

2.Periannan, K., "Evaluation of Occupant Dynamic Responses and Development of Injury Criteria for a 3 Year Old Child," M.S. Thesis, Wichita State University, 1994.

TABLE 1.1 - RESPONSE AT 19G DECELERATION PULSE WITH SEAT AT 60^0 PITCH

	Test	SOMLA/TA	MADYMO	ATB
HIC	97.7	157.7	59.3	151.3
Lumbar Load	1500	2356	1712	

TABLE 1.2 - RESPONSE AT 26G DECELERATION PULSE WITH SEAT AT 60^0 PITCH

	Test	SOMLA/TA	MADYMO	ATB
HIC	252	381	1005	294
Lumbar Load	3327	2755	1902	

TABLE 1.3 - PEAK HIC AT 15G DECELERATION PULSE WITH SEAT AT 10^0 YAW

	Test	SOM-LA/TA	MADYMO	ATB
HIC	54.0	201.0	60.4	47.9

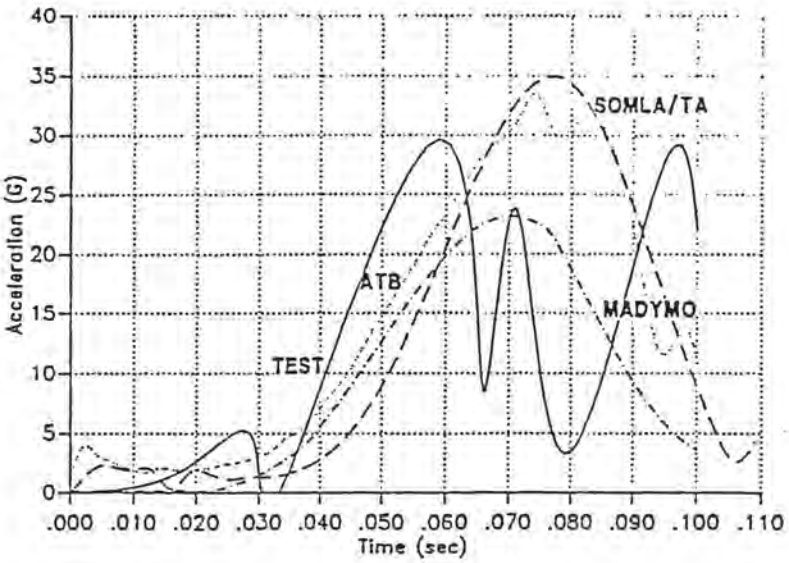

FIGURE 1.1 RESULTANT HEAD ACCELERATION AT 19G PULSE WITH SEAT AT 60° PITCH

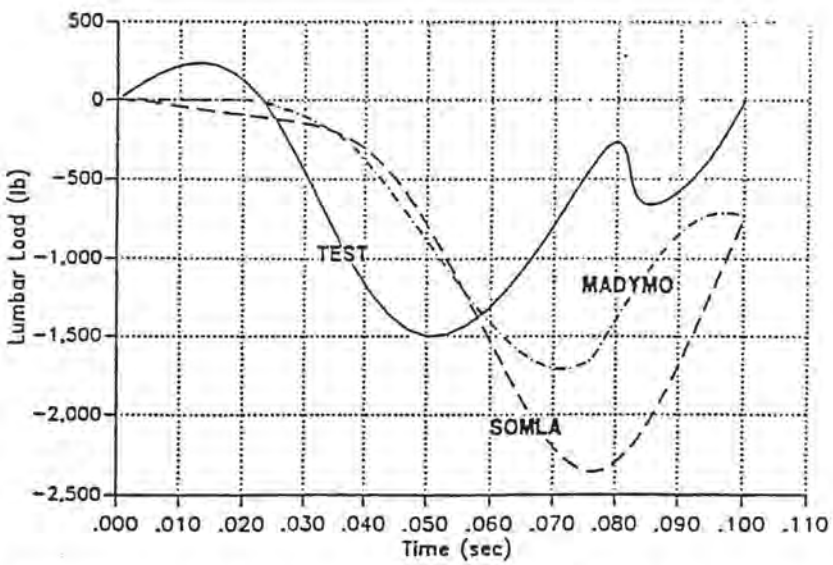

FIGURE 1.2 LUMBAR LOAD AT 19G PULSE WITH SEAT AT 60° PITCH

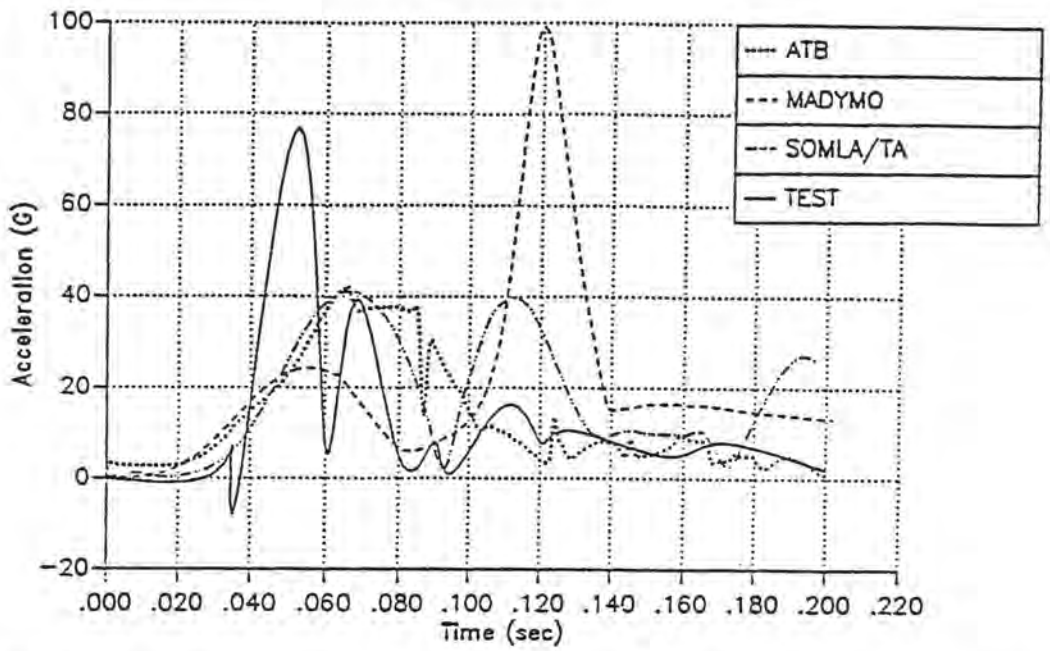

FIGURE 1.3 RESULTANT HEAD ACCELERATION AT 26G PULSE WITH SEAT AT 60^{0}PITCH

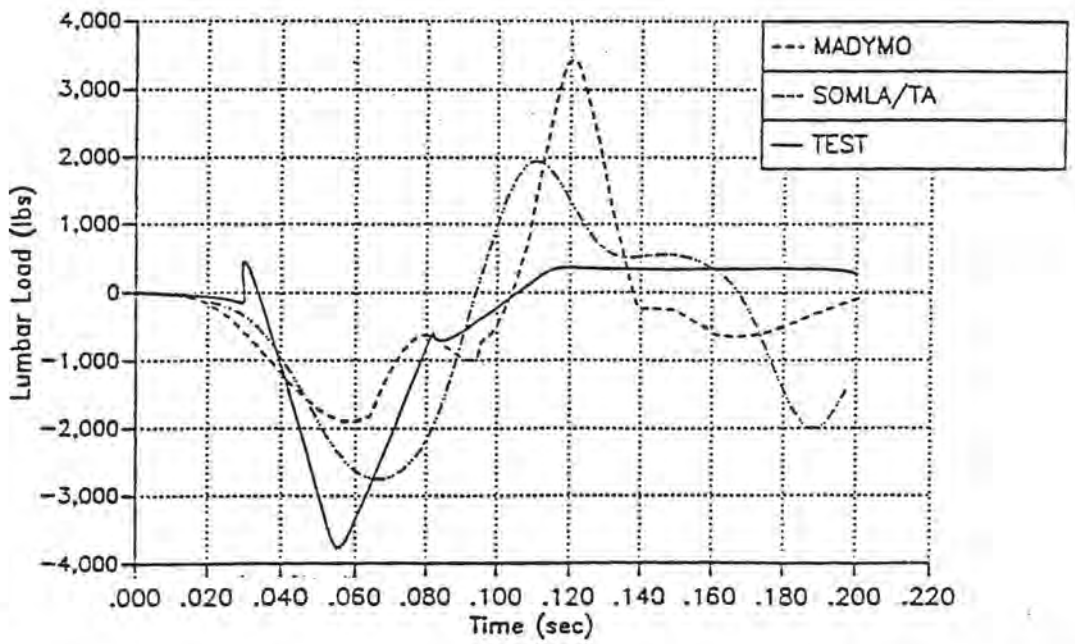

FIGURE 1.4. RESULTANT LUMBAR LOAD AT 26G WITH SEAT AT 60^0 PITCH.

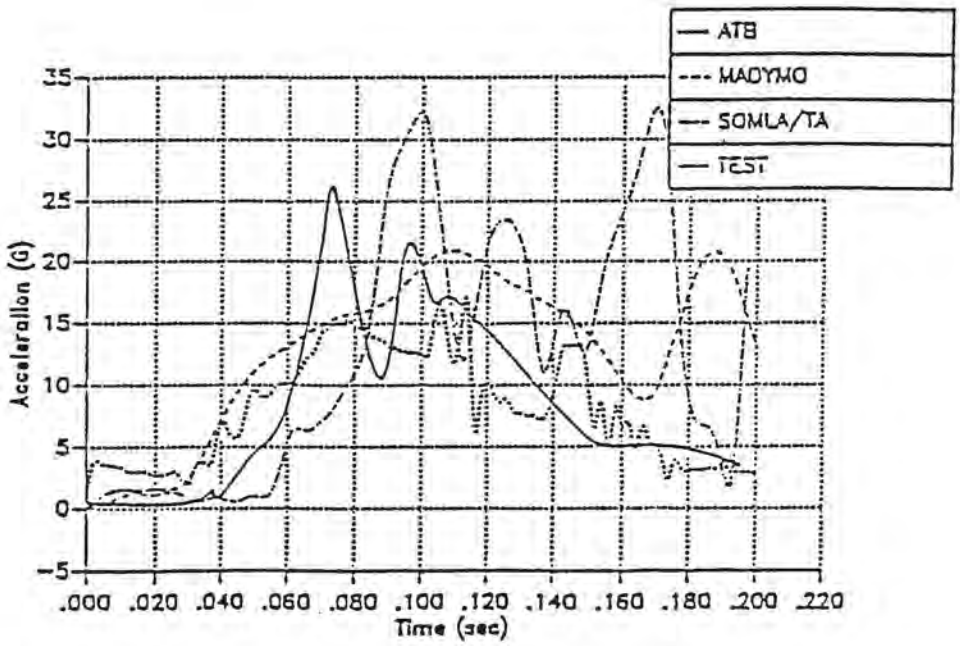

FIGURE 1.5 RESULTANT HEAD ACCELERATION AT 15G PULSE WITH SEAT AT 10^0 YAW

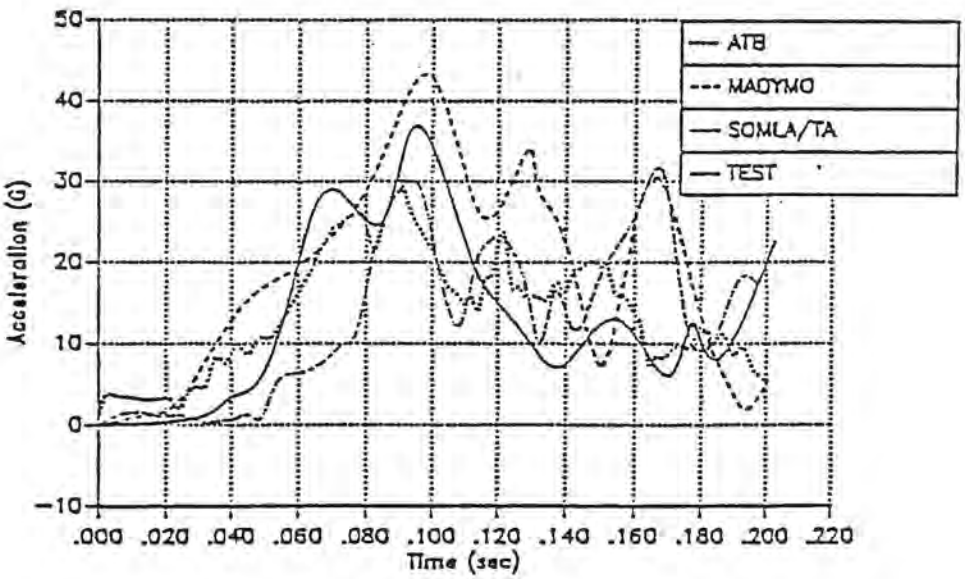

FIGURE 1.6 RESULTANT HEAD ACCELERATION AT 19G WITH SEAT AT 10^0 YAW

2. OCCUPANT RESPONSE WITH A FLEXIBLE LUMBAR SPINE MODEL

2.1 Introduction

Analysis of occupant response carried out using the code SOM-LA/TA has the drawback of modelling the body segments as rigid. This results in inaccurate results for the injury criteria. An improvement in the performance of this code was achieved by modelling the spine as a flexible body [1]. This modified code, referred to as SOM-LA/FEA was found to predict occupant response closer to the experimental results compared to the SOM-LA/TA.

2.2 VALIDATION OF SOM-LA/FEA

In order to provide validations to the program SOMLA-FEA [1], which is a modified version of SOMLA/TA with a finite element lumbar spine, a series of sled dynamic tests were performed at Impact Dynamics Laboratory at National Institute for Aviation Research (NIAR). The experimental tests were set up to comply with Federal Aviation Regulation (Part 23_Test_1 Crew). The GA iron crew seat was used with 60^0 pitch from the plane of the sled as shown in Figure 2.1. The occupant selected was a 50th-percentile (part 572) male dummy. The deceleration pulse was of a triangular shape with a maximum value of 19 G and a span of 100 ms. The impact velocity was 42 ft/sec.

The lumbar spine loads acting on the dummy were digitized and compared with the simulation results as illustrated in Figure 2.2. It is observed that the peak values are 1500 lb from test, 2760 lb from simulation of SOM-LA/TA, and 1930 lb from the simulation of SOMLA-FEA. As to Head Injury Criteria (HIC), the SOMLA-FEA obtained a value of 101.1, which is close enough to the test HIC value 97.7, while the SOM-LA/TA obtained a HIC value of 219.1. The comparison of head resultant accelerations is shown in Figure 2.3. The peak values both from test and simulation of SOMLA-FEA are almost same, while the patterns have some differences. The test result shows that the head resultant has a high acceleration frequency during the period time 60-90 ms. This is probably because that a high frequency filter 1000 Hz was used for data acquisition in the impact sled test and a lower filter 300 Hz in the simulation. The relationship of resultant accelerations among dummy's head, chest and pelvis is shown in Figure 2.4. The other important fact is that the lumbar spine is not only subjected to the axial loads and bending moments, but also the shear forces. Figure 2.5 shows the shear forces as a function of time. It has a similar patten to that of deceleration pulse, and has a peak value of 1500 pounds, which is the same order as the axial forces.

2.3 References

1. Ma, D., "A Multibody/Finite Element Analysis approach for modeling of crash dynamic responses," Ph.D dissertation, Department of Mechanical Engineering, NIAR report 94-3, WSU

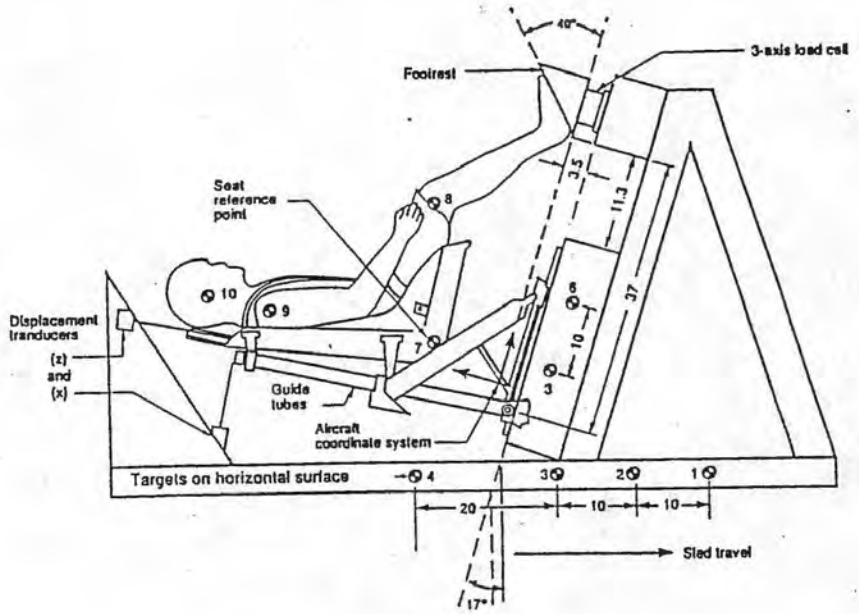

FIGURE 2.1 CONFIGURATION OF SETUP

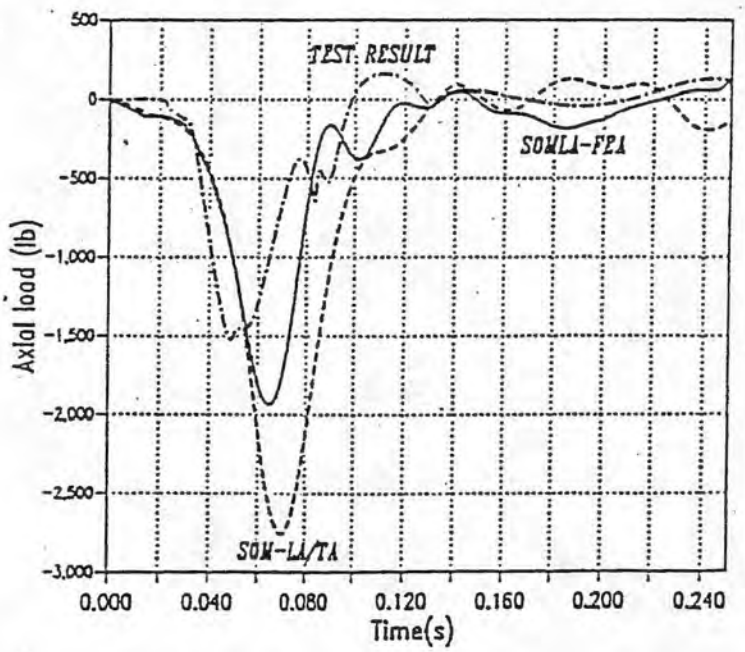

FIGURE 2.2 LUMBAR SPINE AXIAL LOADS

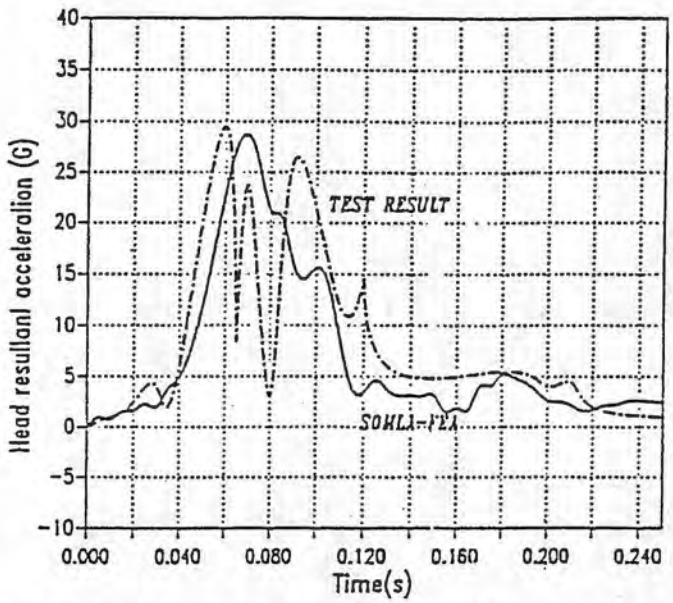

FIGURE 2.3 COMPARISON OF HEAD RESULTANT ACCELERATION

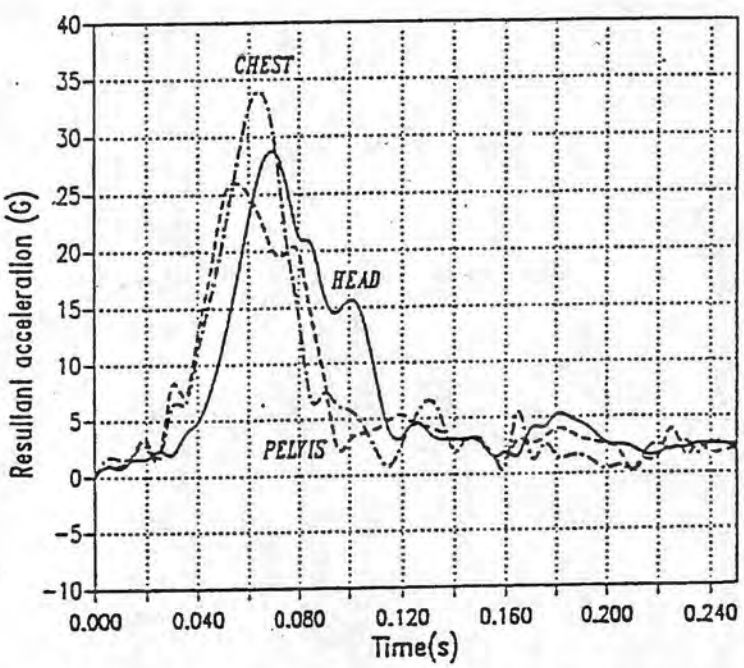

FIGURE 2.4 COMPARISON OF HEAD, CHEST AND PELVIS RESULTANT ACCELERATIONS

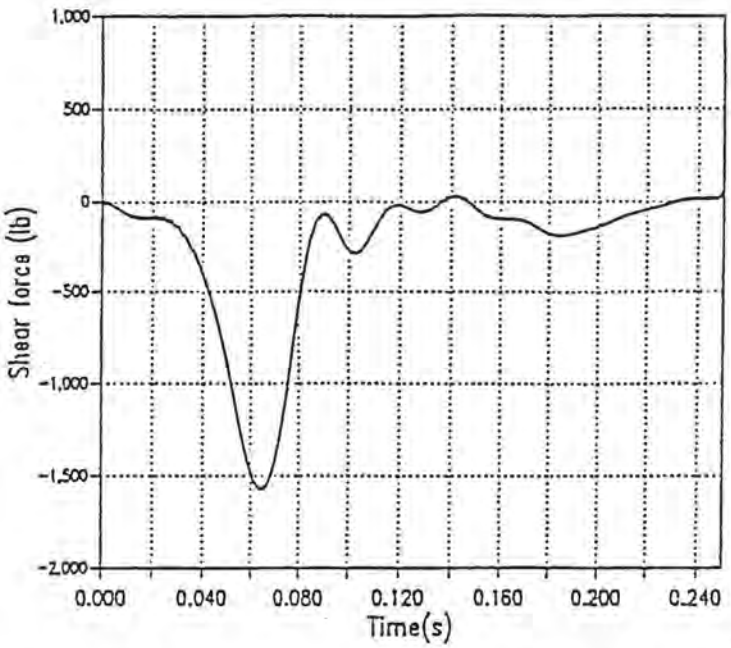

FIGURE 2.5 SHEAR FORCE ACTING ON THE LUMBAR SPINE

3. PADDING MATERIAL SELECTION FOR REDUCING HEAD INJURY

3.1 Introduction

A study was carried out to reduce the risk of occupant's head injury as a result of head impact onto chairs, interior walls, bulkheads, etc. by establishing a reasonable procedure for the selection of required clearances and padding materials. The response of human head as well as the padding material were investigated by finite element analysis.

All the analyses were conducted using the explicit, nonlinear dynamic finite element program COSMOS/M (version 1.70). The contact/impact of the head with the panel and padding surface was investigated.

3.2 Finite Element Model

The finite model of the head impacting a surface was built using 8 noded brick elements as shown in Figures (3.1) and (3.2). To simulate the contact, the head and the impact surface were connected with gap elements. An initial velocity was specified for the head while the impact surface was held stationary. The back of the impact surface was fixed rigidly to simulate rigid backing behind the padding material. The padding material investigated was rigid foam with Yield strength and Young's modulus of 11 kPa and $5*10^5$ Pa respectively. A value of 0.49 for Poisson's ratio and 30 kg/mm^3 for density was used for the padding material. For the head, a value of $6.5*10^9$ Pa was assigned for Young's modulus, 0.22 for Poisson's ratio and 1150 kg/mm^3 for density.

3.3 Validation of the Methodology

To validate the methodology, a preliminary analysis was conducted to duplicate the results of "Bowling Ball Drop Tests" (as defined in AC 25-17) carried out by the Biodynamic Research section of the FAA Civil Aero Medical Institute (CAMI) [1]. In this test a bowling ball was used to simulate the head impact of a 170 pound occupant. The bowling ball was instrumented. Tests were conducted by raising the ball to the desired height by means of a pulley as shown in Figure (3.3). Upon manual release the ball drops freely on the test specimen. After impact, the maximum rebound velocity of the bowling ball and the indentation response on the padding material were recorded using a high speed video camera. Later these data were used to calculate the peak acceleration in G's and the HIC value. An impact velocity of 36 ft/sec consistent with sled tests specified by FAR 25 was given to the head and allowed to impact on the padding material under test. Figure (3.4) shows the acceleration response of head with time during the crush along with the test results. It may be noticed that the peak value of the acceleration from the analysis is in close agreement with the test result. HIC calculated from the analysis was found to be 1212 where as the HIC from the test results was 1230. The contact force - indentation response is shown in Figure (3.5). It is seen to be highly nonlinear. The analysis was extended further for simulating head impact with different padding materials.

3.4 Head impact onto Ideal and Rigid Foam

An ideal padding material is one which yields instantaneously under the application of load with no elastic deformation. Thus an ideal material provides a constant deceleration pulse. Rigid foam exhibits elastic deformation before yielding. The rigid padding material was assigned an Yield strength and Young's modulus of 11.0 kPa and 0.5 MPa respectively. A value of 0.49 for Poisson's ratio and 30.0 kg/mm^3 for density was used for the padding material. As before, for the head, a value of 6.5 GPa was assigned for Young's modulus, 0.22 for Poisson's ratio and 1150 kg/mm^3 for density.

The deceleration response of the head during the crush of the padding material is shown in Figure (3.6). It may be noticed that the Ideal material provides a constant deceleration pulse where as the Rigid foam provides a deceleration pulse varying with time. Figure (3.7) shows the velocity response for Ideal and Rigid foam. The change in velocity is uniform for Ideal material and is not uniform for Rigid foam. The indentation response is shown for Ideal and Rigid foam in Figure (3.8). The rigid foam initially gets deformed to a maximum value during the compression phase of impact and during the restitution phase, attains a permanent deformation.

The analysis was continued further and a few more conclusions were drawn. As seen from the velocity response, Figure (3.7), the head bounces back with a velocity of 4 m/s for rigid foam impact. The total change in velocity Δv is 15 m/s. It can be seen from Figure (3.8) that the maximum deformation is 0.123 m. This can be shown to be approximately equal to the theoretical crush value as discussed below.

3.5 Calculation of theoretical crush

The equation for HIC can be written as

$$HIC = (t_2 - t_1)\left[\frac{1}{(t_2 - t_1)}\int_{t_1}^{t_2} a(t)dt\right]^{\frac{5}{2}} \qquad (3.1)$$

where t_1 and t_2 are chosen to maximize HIC and a(t) is absolute acceleration of the head measured in G's. The analysis for an ideal padding material is explained below.

An Ideal padding material during crush produces a rectangular pulse of deceleration and also the change in velocity is linear. Since the integral of a rectangular acceleration pulse is the change in velocity during the time interval t_2 to t_1, Equation (3.1) can be rewritten as

$$HIC = \Delta t\left[\frac{\Delta v}{\Delta t\ g}\right]^{\frac{5}{2}} \qquad (3.2)$$

where 'g' is the gravitational constant. Again Δv can be expressed in terms of maximum indentation Δx as

$$\Delta x = \frac{\Delta v}{2}\Delta t \qquad (3.3)$$

Combining Equations (3.2) and (3.3) and rearranging the HIC equation yields

$$\Delta x = \Delta v^{8/3} \left[\frac{1}{8(HIC)^2 g^5} \right]^{\frac{1}{3}} \qquad (3.4)$$

Substituting the value of Δv as 15 m/s and HIC as 1212 for Rigid foam head impact, the theoretical value for the maximum indentation can be seen to be 0.133 m [2]. This can be treated to be a fairly close agreement with the value of Δx obtained from Figure (3.8) considering all the assumptions made in the equation. This result can be used for the preliminary selection of the of the padding material as discussed below.

It can be seen that setting HIC to 1000 and g as 9.81 m/s^2 in Equation (3.4) results in

$$\Delta x = \Delta v^{\frac{8}{3}} * 111.2213 * 10^{-6} \qquad (3.5)$$

where Δx is in m and Δv is in m/s. Assuming that the head comes to rest at the end of impact, Δv may be approximated to be equal to the impact velocity v. This indicates that the padding material to be selected should be able to get deformed through Δx when subjected to an impact velocity v. This is shown in Figure (3.9). From the figure the minimum required crush at any given velocity resulting in a HIC of 1000 can be estimated. Accordingly, a suitable padding material satisfying this requirement may be selected.

3.6 HIC response surface

Also, selection of proper padding material is generally reflected in the form of material properties such as Young's modulus, yield stress and plastic deformation contour. Material parameter study was conducted using design of experiments which correlate the HIC and the padding material characteristics in the form of response surface as shown in Figure (3.10). Optimum material property characteristics which minimize the HIC can be obtained from the response surface.

3.7 Conclusions

The analysis predicted the magnitude of maximum and permanent deformation of the padding and maximum indentation force of the head fairly accurately. The results of the test revealed that using finite element techniques the response of the head impact on a padding surface can be predicted fairly accurately.

3.8 References

1. Gowdy, V., "Evaluation of Head Protection Method in Advisory Circular 25-17: The Bowling Ball Test," Draft # 3, Biodynamics Research Station of FAA, Civil Aero Medical Institute, 1993

2. Santhanam, S., "Impact Response of an Anthropomorphic Test Dummy Head using Nonlinear Finite Element Methods," M.S. Thesis, Wichita State University, 1994.

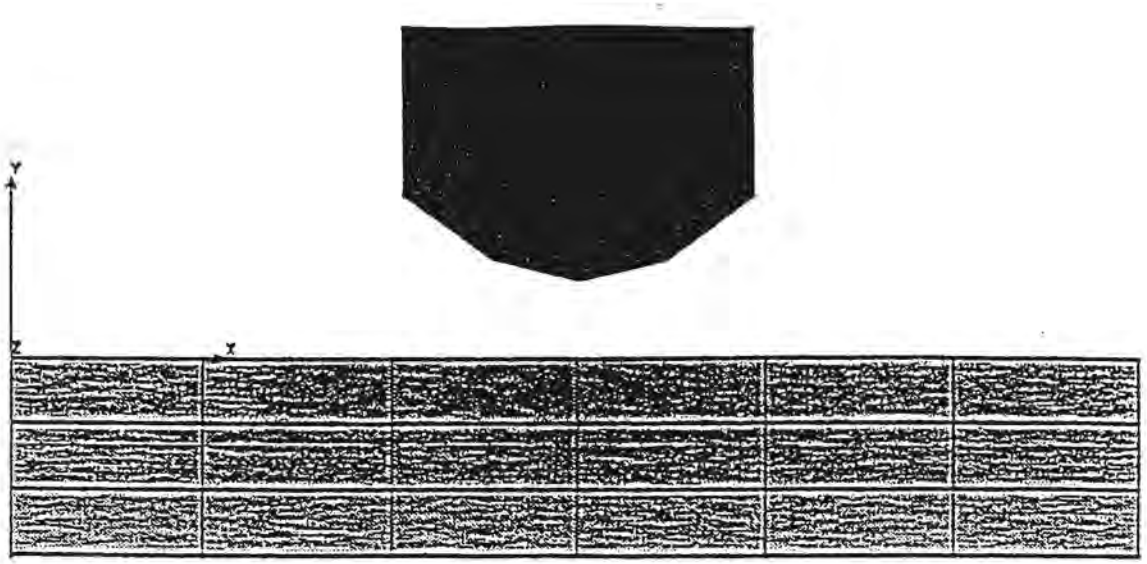

FIGURE 3.1 GEOMETRICAL REPRESENTATION (2D) OF THE FINITE ELEMENT MODEL

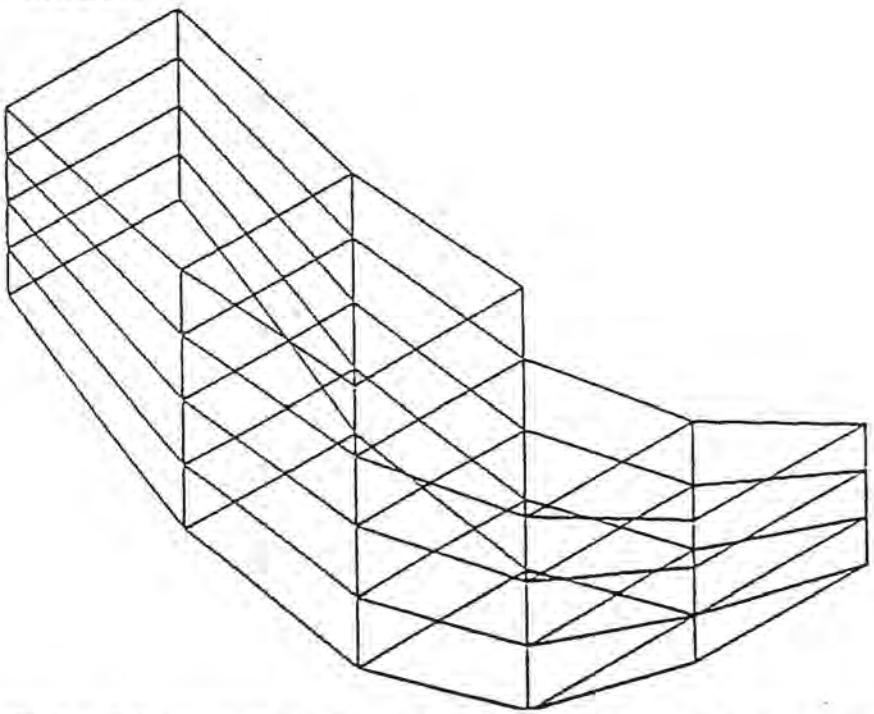

FIGURE 3.2 EIGHT NODDED SOLID BRICK ELEMENT MESH

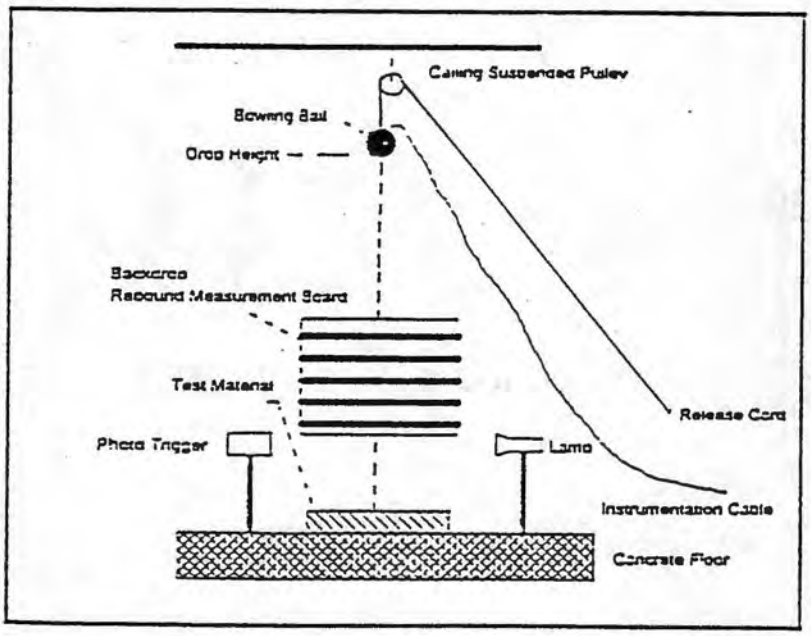

FIGURE 3.3 DROP BALL TEST SETUP

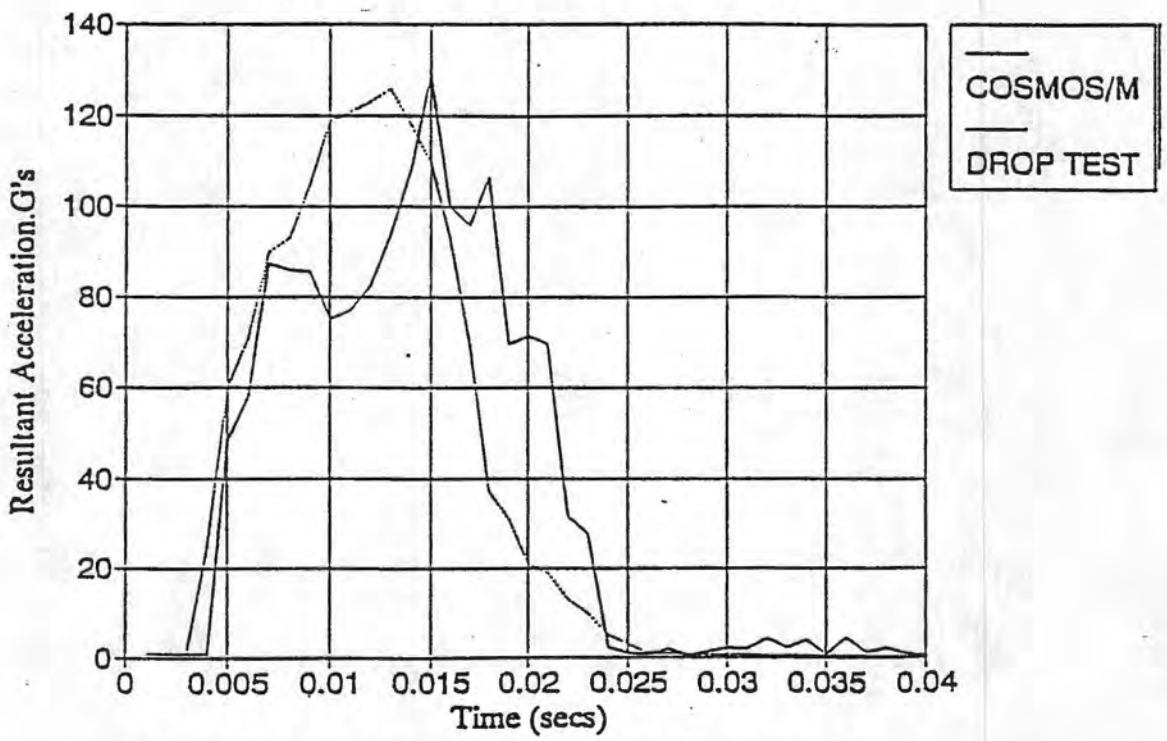

FIGURE 3.4 ACCELERATION RESPONSE OF THE HEAD

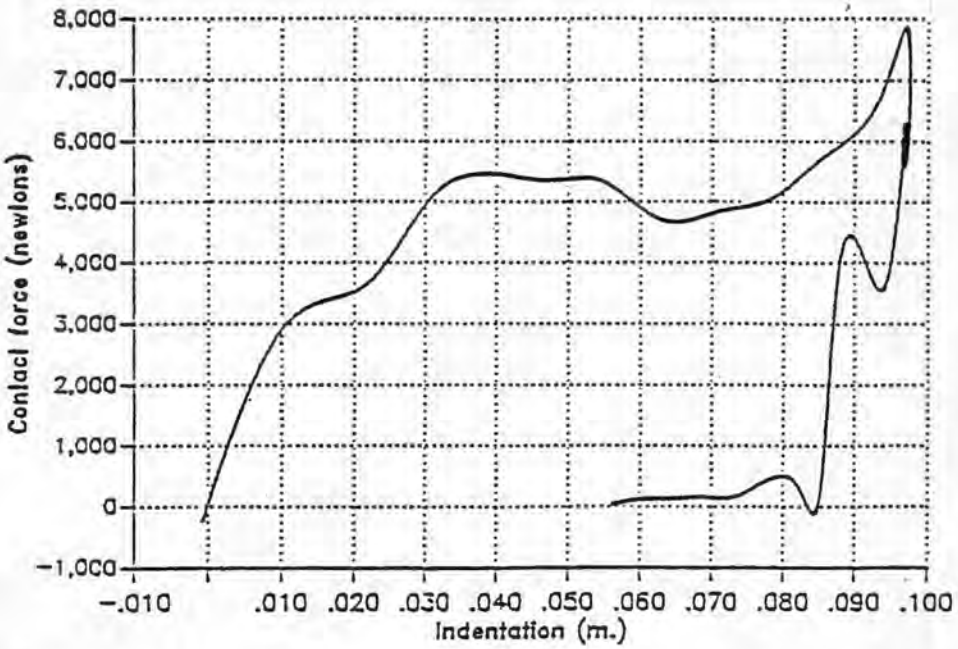

FIGURE 3.5 CONTACT FORCE RESPONSE DURING INDENTATION

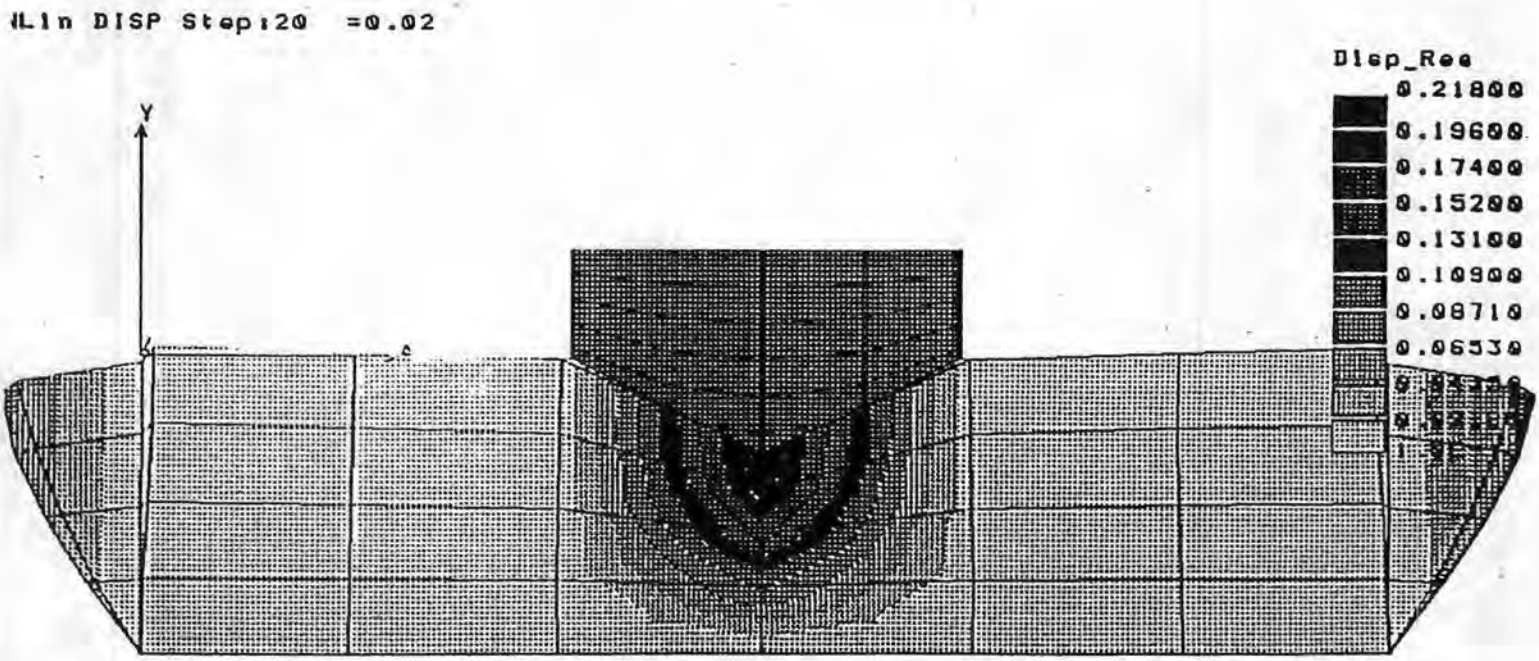

FIGURE 3.6 DISPLACEMENT PLOT DURING HEAD IMPACT

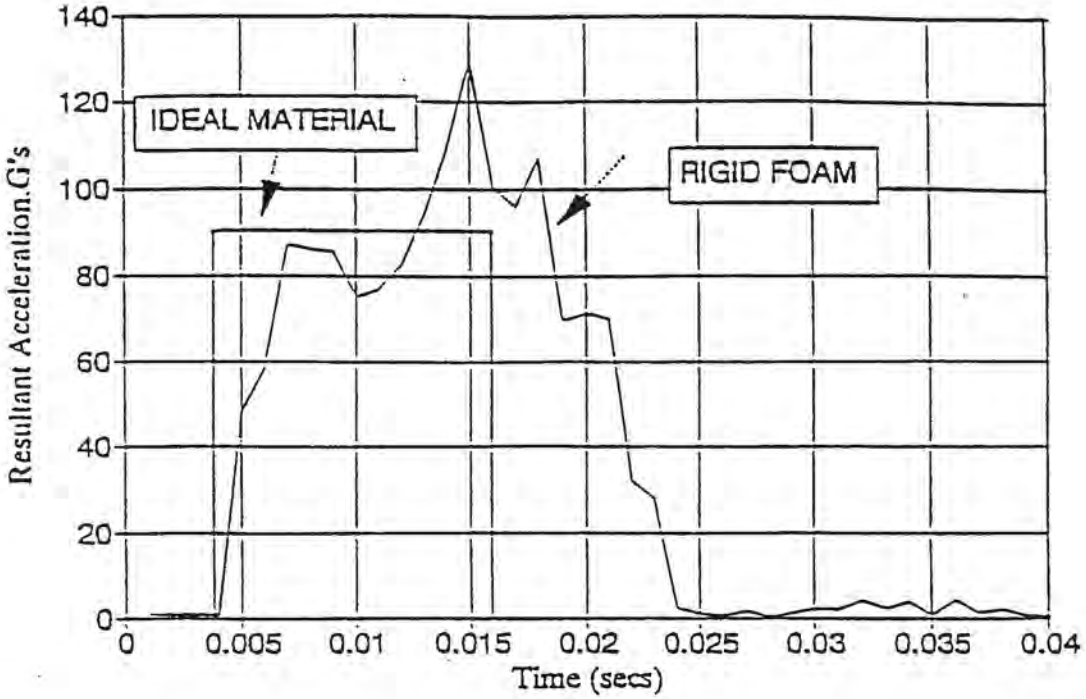

FIGURE 3.7 ACCELERATION RESPONSE DURING IMPACT ON IDEAL AND RIGID FOAM

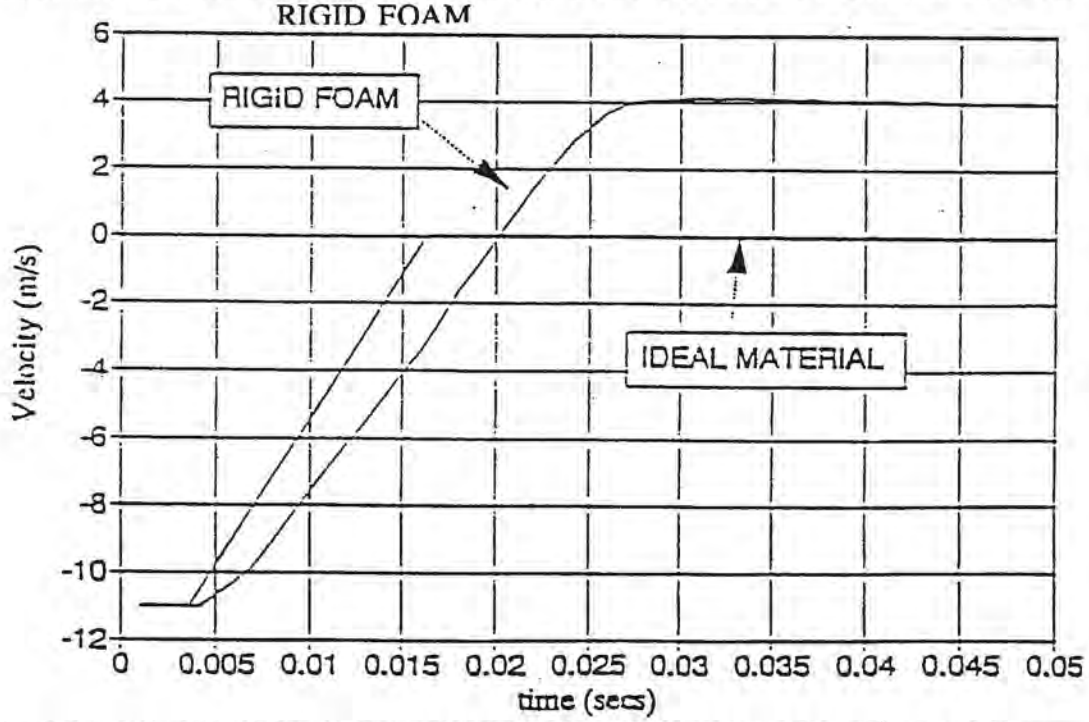

FIGURE 3.8 VELOCITY RESPONSE DURING IMPACT ON IDEAL AND RIGID FOAM

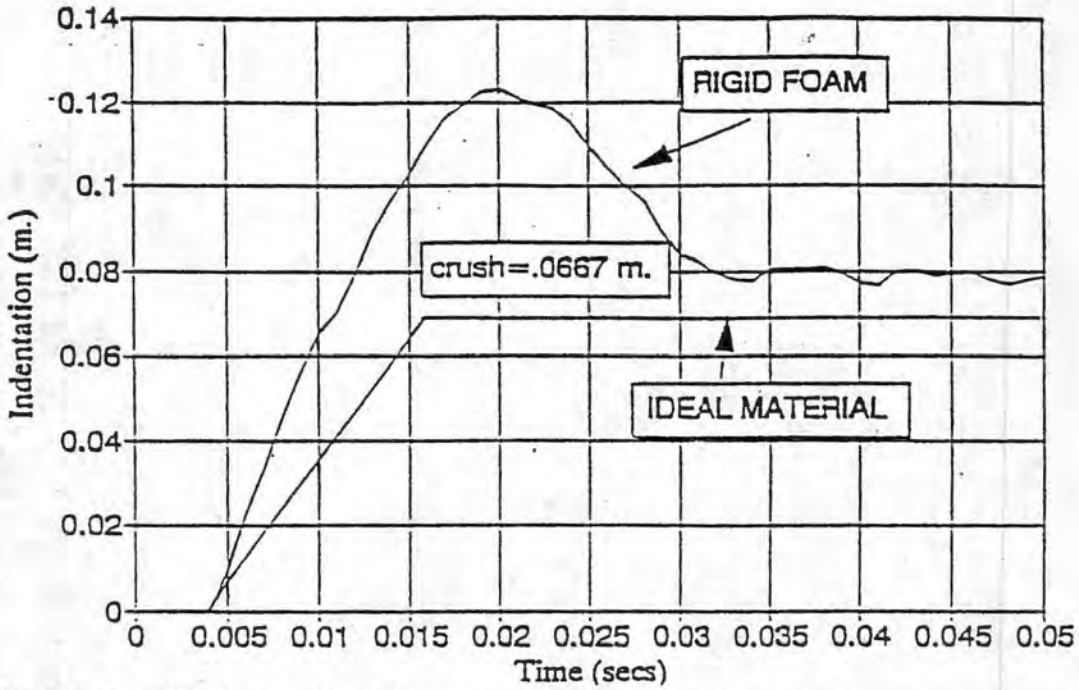

FIGURE 3.9 INDENTATION RESPONSE DURING HEAD IMPACT ON IDEAL AND RIGID FOAM

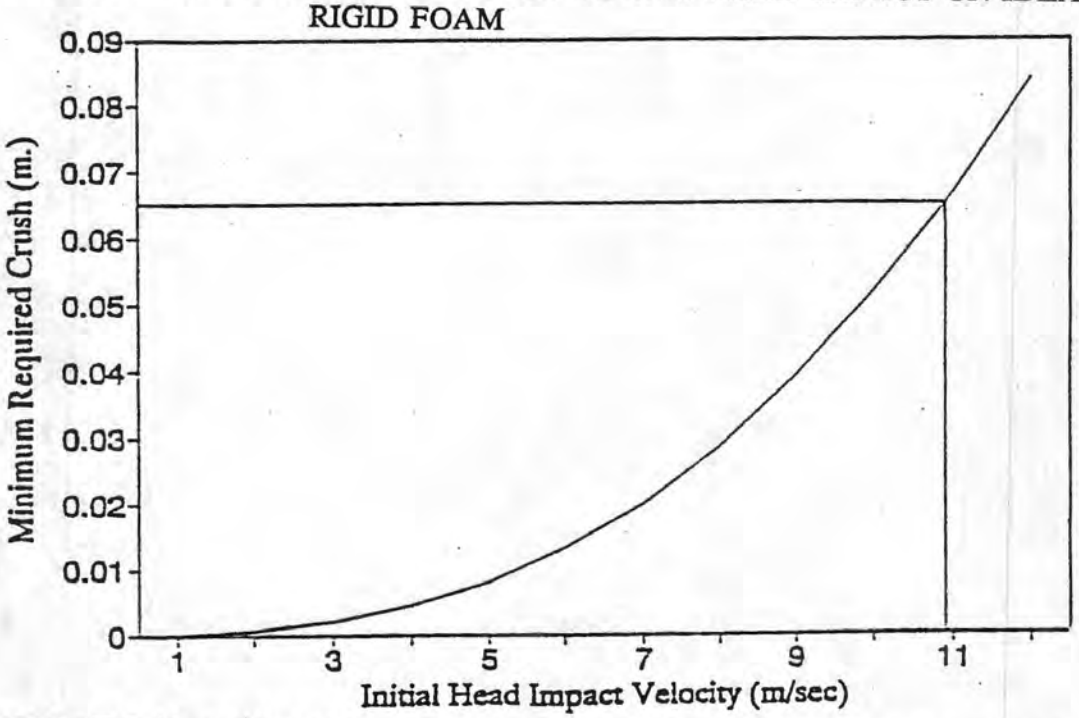

FIGURE 3.10 VARIATION OF MINIMUM REQUIRED CRUSH WITH IMPACT VELOCITY RESULTING IN A HIC OF 1000

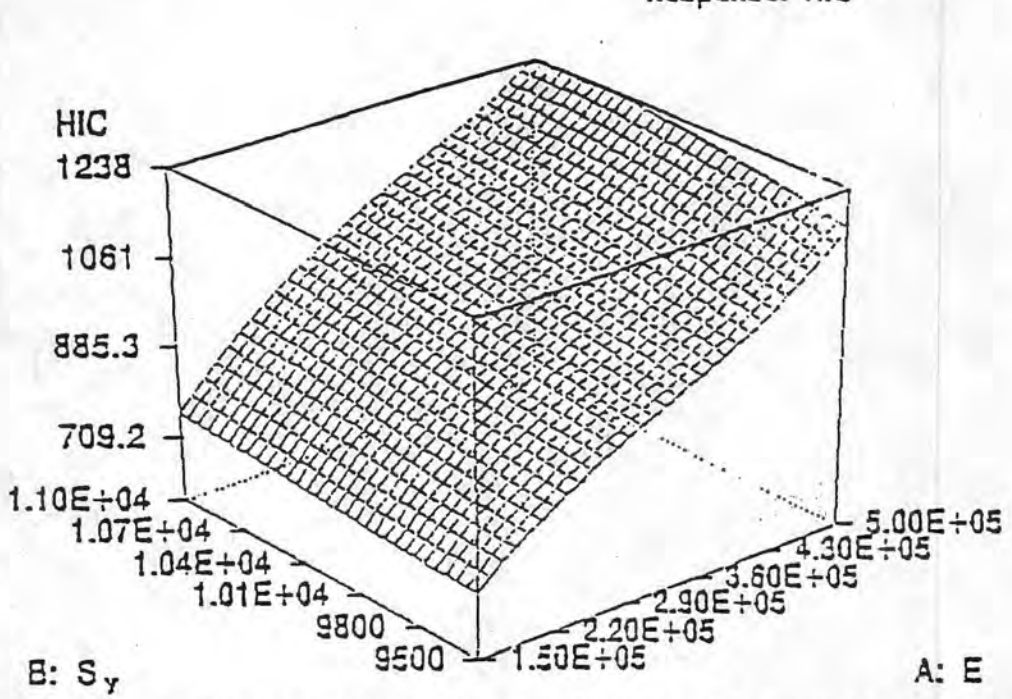

FIGURE 3.11 RESPONSE SURFACE OF YIELD SURFACE (S_Y), YOUNG'S MODULUS (E) WITH HIC

4. NON SLED IMPACT TEST SETUP

4.1 Introduction

Protecting occupants from head injury is one of the most crucial factor in crash worthiness design. Head impact can occur onto the seat in front, bulkheads etc. Lining the potential target areas with padding material helps in reducing injury during head impact. The padding material absorbs the kinetic energy of the head during impact and thus reduces head injury. Thus testing of padding materials is crucial in the selection of optimum padding material in a given crash environment. The tests can be carried out using conventional sled setup. Impact sled tests of the dummy/ seat/ restraint system and the front panel mounted on the sled are costly, time consuming and provide too much scatter or probability of HIC. Alternatively, non-sled testing procedures (component or element testing with the ATD head only) were developed for this project, that are more controllable, more repeatable, less time consuming and less costly. Hence, the design and fabrication of non sled type test setup was carried out. The nonsled setup apart from being economical are easy to operate and maintain with very little operating cost. The fabrication cost of a nonsled test setup will be less than 1/10 th of the conventional sled setup [1]. Three different types of setups were considered for the purpose. They are

a. Drop tower type (Figure 4.1)
b. Pneumatic type (Figure 4.2)
c. Pendulum type (Figure 4.3)

Drop tower setup is simple in construction but is not flexible as the pendulum type. In the drop tower setup, the head is raised to a height and then dropped onto the surface to be tested. In the pneumatic type, the head is attached to a piston which is driven inside a cylinder with high pressure gas. In the pendulum type, the head is attached to a pendulum and raised to the desired height and dropped freely to strikes the target at the desired velocity. The pendulum setup has the advantage of being simple in construction and flexible in operation and was considered. Also, with a pendulum test setup, both the padding material and the individual body components can be tested. This can be used for simulating the impact of an occupant onto the interior or the impact on a pedestrian.

4.2 Pendulum Impact Test Setup

The design of the Head Strike Test Rig (HSTR) is shown in Figure (4.3). This new test rig is setup at the west end of the NIAR Impact Dynamics Laboratory behind the deceleration zone. The entire setup will be hooked on to the cross over head beam. The aluminum pendulum was fixed to the shaft with roller bearings. The overall structure consists of one main striking pendulum which is brought to rest by an other small pendulum (motion arrestor). The total length of the main striking pendulum is 20 feet. When released from maximum height, the pendulum will be theoretically is capable of attaining a maximum velocity of 50 ft/sec at its end. The small pendulum connected to shocks will facilitate in absorbing the energy of the pendulum system. An electrically controlled latch mechanism coupled with an infrared sensor is used for sensing the dummy and release the padding material at the time of

impact so as isolate the kinetic energy of the pendulum onto the dummy.

To the main pendulum, a panel/ dummy head is fixed loosely as shown in Figures (4.4) and (4.5). The padding material to be tested will be mounted on the panel. During the course of travel of the main pendulum, the dummy head comes in contact with the padding material and gets detached from the pendulum (Figure 4.4). This eliminates the inertial forces of the pendulum being transferred to the dummy head. With a suitable arrangement, the dummy head will be stopped before hitting the ground. After the impact, the pendulum will travel freely until it comes in contact with the small motion arrestor pendulum. A couple of solenoid locks fixed on the motion arrestor pendulum which will lock the two pendulums. After this, the two pendulums move as a single unit and the energy of the system will be dissipated by the shocks.

The test can be conducted at any desired velocity by suitably adjusting the inclination of the pendulum. The relationship between the impact velocity and the inclination can be obtained using energy relations as

$$V = \sqrt{(2gh)}\,, \qquad h = l\,(1 - \cos\theta) \tag{4.1}$$

where l is the length of the pendulum and θ is the inclination of the pendulum with the vertical as shown in Figure (4.6).

The entire process will be recorded with high speed cameras for further image processing. Accelerometer and other transducers will be mounted on to the dummy as well as the main pendulum which will be further connected to a data acquisition system.

With the help of this setup, the effect of stiffness of the padding material on the value of HIC can be studied. A satisfactory model of head impact with nonlinear stiffness and damping properties of padding material can be developed once the preliminary results are available. This helps in the selection of optimum material for reducing severe head injuries.

4.3 Design Methodology

The whole design process of the setup can be summarized as follows.

a. Determine the stiffness and damping properties of the shocks.
b. Select a suitable cross section and material for the pendulum.
c.. Conduct a Finite Element Analysis and check whether the stresses are less than the yield stress.
d. Conduct a rigid body analysis for the system to find out whether the maximum deflection of the shocks during the impact is less than it's stroke, otherwise the shocks fail.
e. If failure is encountered, select a new suitable cross section and material and carry out the analysis once again.

4.4 Testing of Shock absorber

Compression tests on the shocks were carried out in order to evaluate the stiffness and damping properties since these were not available. These values are required in the stress analysis to find out whether the pendulum beam can withstand the high stress during the deceleration of the beam. The shocks were tested in a universal testing machine at the

structures laboratory.The shocks were fixed rigidly to the jaws of the machine and was compressed at an uniform rate. Displacement and the reaction force offered by the shocks during the compression were recorded and the results are described below.

During the analysis, it was found that the damping property of the shocks was dominant compared to the stiffness and hence it was ignored in the calculations. The damping coefficient was calculated from the ratio of the reaction force to the displacement rate.

Figure (4.7) shows the variation of damping coefficient during compression at a displacement rate of 1.3 in/sec. It might be seen that the damping co-efficient value varies slightly during the compression and the average value was found to be 26.62 lbf-sec/in.

Figure (4.8) shows the variation of damping coefficient with displacement for a displacement rate of 4.75 in/sec. The average value was found to be 13.05 lbf-sec/in. The value of the damping coefficient varies slightly during compression.

Figure (4.9) shows the values of damping coefficient at different velocities. It was found that the value of damping co-efficient decreases rapidly in an exponential manner with increase in displacement rate.

4.5 Finite Element Analysis

Finite element analysis of pendulum head impact test rig was carried out using NASTRAN. The aim of the analysis is to find out whether the selected cross section and material for the pendulum beam can withstand the stresses during the deceleration before it comes to rest due to the damping.

The finite element model consisted of nine bar elements and ten node points as shown in Figure (4.10). An initial velocity was specified at all the nodes to simulate the impact conditions. All the nodes were constrained not to move in the Z direction. Also the rotations about X and Y axes were constrained. At the pivot point, displacements about X and Y axes were constrained. The maximum value of nodal stresses during the deceleration were noted down and checked for yielding of the pendulum.

A number of trials were run varying the cross section and the damping value to ensure that neither the beam is stressed beyond the yield point nor the shocks get bottomed out. Also, the effect of introducing reinforcement at the high stressed regions were analyzed. Some of the details of the analyses are presented here.

Figure (4.11) shows the results for Steel 3 in X 2.0 in 0.25 in thick I-section. The shocks were assumed to be fixed at a distance of 4 ft from the hinge with a damping value of 10 lbf-sec/in. It can be seen that the stress at node 3 is greater than the yield stress. It is concluded that section will fail.

To strengthen the beam, a reinforcement in the form of 0.5 in thick plate was added to the cross section at the high stressed zone (from 2 ft to 10 from the hinge point). This resulted in a low value of stress as shown in Figure (4.12). However, the section was very heavy and hence possessed a high inertia. As a result of this, it was observed from the rigid body analysis that the motion of the pendulum can not be restricted with in the safe region and hence the shocks would get bottomed out. In the rigid body motion analysis, the differential equations of motion of the system are solved for displacement, velocity and acceleration. To restrict the motion of the pendulum beam, a high value of damping was introduced in the analysis. This

simulates the use of multiple shocks for absorbing the kinetic energy of the pendulum beam. This resulted in high stresses in the pendulum beam. The results are shown in Figure (4.13). It can be concluded that the selection of cross section with the reinforcement is not safe.

A 0.25 in thick 3x2 in rectangular cross section steel beam with a reinforcement of 0.5 in thick plate from 2 ft to 12 ft from the hinge point was tried out. The shocks were modelled as a damper with damping value of 20 lbf-sec/in at a distance of 6 ft from the hinge. It was noticed that the stresses were high even though the shocks were safe from getting bottomed out. Then, a 0.25 in thick 4x2 rectangular cross section steel beam with a reinforcement of 0.5 in plate from 2 ft to 12 ft was tried out. This again resulted in high stress as seen in Figure (4.13). From all the analyses it can be concluded that the main reason for failure is because of the large inertia associated with the pendulum. Therefore, the finite element analysis was continued with aluminum cross section. Selection of aluminum has the advantage of being light and hence low inertia compared to the steel section. A 0.25" thick 3x2 C channel aluminum beam was tried. A damping value of 10 lbf-sec/in was introduced in the analysis. The resultant stress distribution along the length of the beam was below the yield point and hence the beam is safe from yielding. The rigid body dynamic analysis was also carried out to find out the displacement response of the system to ensure that displacement of the shocks are well within the stroke limits. It was observed from the analysis that the maximum displacement of the beam is 0.1 radian for aluminum cross section. This at the shocks, which is at a distance of 4 ft from the hinge corresponds to a linear displacement of 5 in. Since the safe displacement of the shocks was found to be 8 in, it can be concluded that the shocks do not fail for aluminum beam. Further, aluminum rectangular cross section of 3x2 was tried out with a damping value of 10 lbf-sec/in. It was found that the stresses were less than the yield point stresses and shocks were safe from getting bottomed out. So, it was concluded that aluminum C-channel should be used for safe operation. The overall results are summarized in Table 4.1.

TABLE 4.1 SUMMARY TABLE

Material	Cross Section	Yield	Damping Value & Distance from hinge	Shock Fail
Steel	3x2x.25(Rect)	Yes	10 lbf-s/in @ 4 ft	Yes
Aluminum	3x2x.25(Rect)	No	10 lbf-s/in @ 4 ft	No
Aluminum	3x1.75 c-channel	No	10 lbf-s/in @ 4 ft	No
Steel(Rein)	3x2x.25(*)	No	10 lbf-s/in @ 4 ft	Yes
Steel(Rein)	3x2x0.25(**)	Yes	20 lbf-s/in @ 6 ft	No
Steel(Rein)	4x2x.25(**)	Yes	20 lbf-s/in @ 6 ft	No

(*)-Reinforcement with 0.5" plate on both sides from 2 to 10 ft from hinge
(**)-Reinforcement with 0.5" plate on both sides from 2 to 12 ft from hinge

4.6 Fabrication Details

The view of the pendulum setup at NIAR crash lab is shown in Figure (4.14). The whole assembly is setup beyond the deceleration zone of the horizontal sled.A detailed layout of the setup is shown in Figure (4.15). The lifting arm which is attached to the pendulum structure has been erected. The braking system which consists of shock absorber and rubber bumpers mounted braking pendulum has been fabricated. The pendulum is Aluminum C - Channel. Aluminum channels of smaller lengths was bolted together to obtain the required length. The other details of the fabrication are shown in Figures (4.16) - (4.22). Figure (4.16) shows the overall configuration details of test setup. The details of the fixture of the impactor and arrestor pendulum can be seen in the figure. The two pendulums are hooked to the support structure by 1" diameter solid steel shaft. The pendulum will be raised to the position with the help of hoist winch motor system and released from the desired position. The position of the pendulum is sensed by a transducer. The impactor pendulum is brought to rest by the motion arrestor pendulum with shocks which absorb the kinetic energy. Figure (4.17) and (4.18) show the details of the lift arm. The lift arm is bolted onto the impactor pendulum. This is pulled by the hoist winch mechanism. Figure (4.19) and (4.20) reveal the details of the impactor pendulum. The overall length of the pendulum is 19 ft. A board with padding material will be fitted loosely at the end of the pendulum which gets detached after coming in contact with the dummy. Figure (4.21) and (4.22) show the details of the motion arrestor pendulum system. It has a length of 7 ft 2 in. It has rubber bushes at the point where the impactor pendulum comes in contact with it. This helps in reducing the shock on the system. After the contact occurs between the two pendulums, they move as a single unit. The shock absorber attached dissipates the kinetic energy of the system.

4.7 Results from Trial Test

A preliminary trial test was conducted with the setup to check the accuracy of the instrumentation. In the test , the pendulum with 1" thick CONFOR CF-42 padding material bonded on a panel board of 6 lb weight, was released from 30^0 resulting in a theoretical velocity of 12.76 ft/sec as shown in Figure (4.4). Using the Ektapro motion analyzer, a velocity of 11.93 ft/sec was measured. The difference may be attributed to the drag forces and small inaccuracies that might have been present measuring the inclination. The acceleration pulse on the dummy head was recorded with accelerometers in the X, Y, Z directions. The resultant acceleration response of the head is shown in Figure (4.23). A HIC of 748 was obtained. This is a high value for the velocity at which the test was conducted. This was due to the bonding of the panel board to the pendulum firmly with duct tape, due to which the panel was not allowed to impact the dummy freely, but carry a part of the inertia of the pendulum. This resulted in the transfer of the kinetic energy of the pendulum to the dummy head. However, with the use of infrared sensing latch mechanism as shown in Figure (4.3) , the kinetic energy of the pendulum can be isolated from getting into the system.

4.8 References

1. Sanjeev, A., Lankarani, H.M., "Design of a Non Sled Setup to measure Head Injury Criteria," NIAR Report 92-20, Wichita State University.

2. Sanjeev, A., " Design and Analysis of Head Component Testing Mechanism to Evaluate HIC and Padding Material Performance," M.S. Thesis, Wichita State University, 1994.

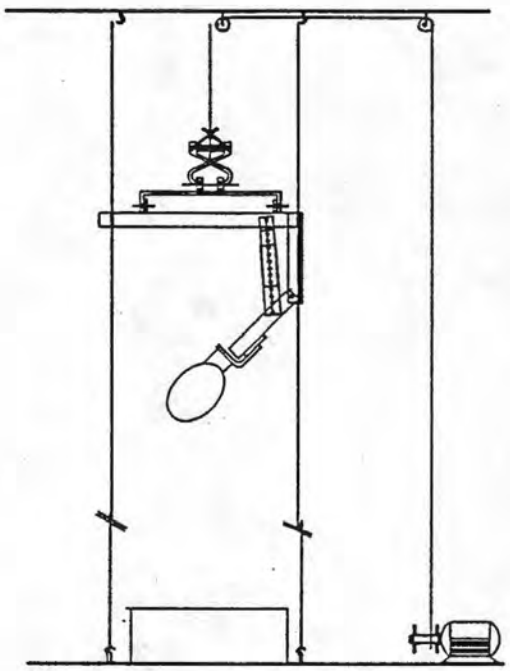

FIGURE 4.1 DETAILS OF DROP TOWER TEST SETUP

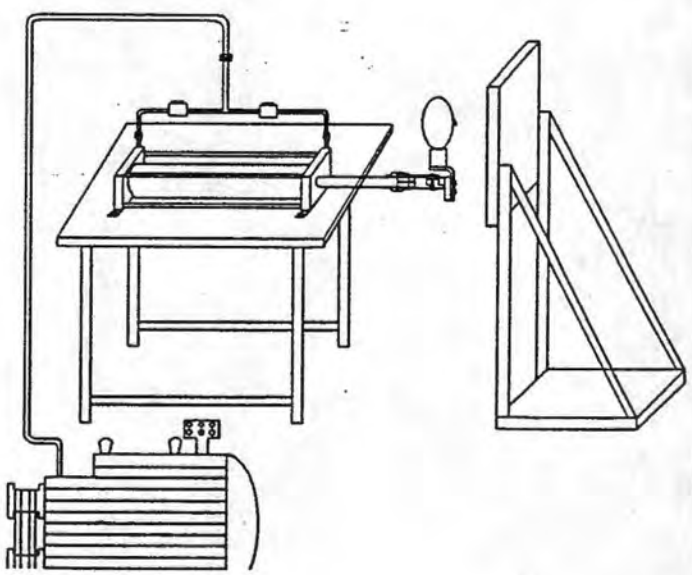

FIGURE 4.2 DETAILS OF PNEUMATIC TYPE TEST SETUP

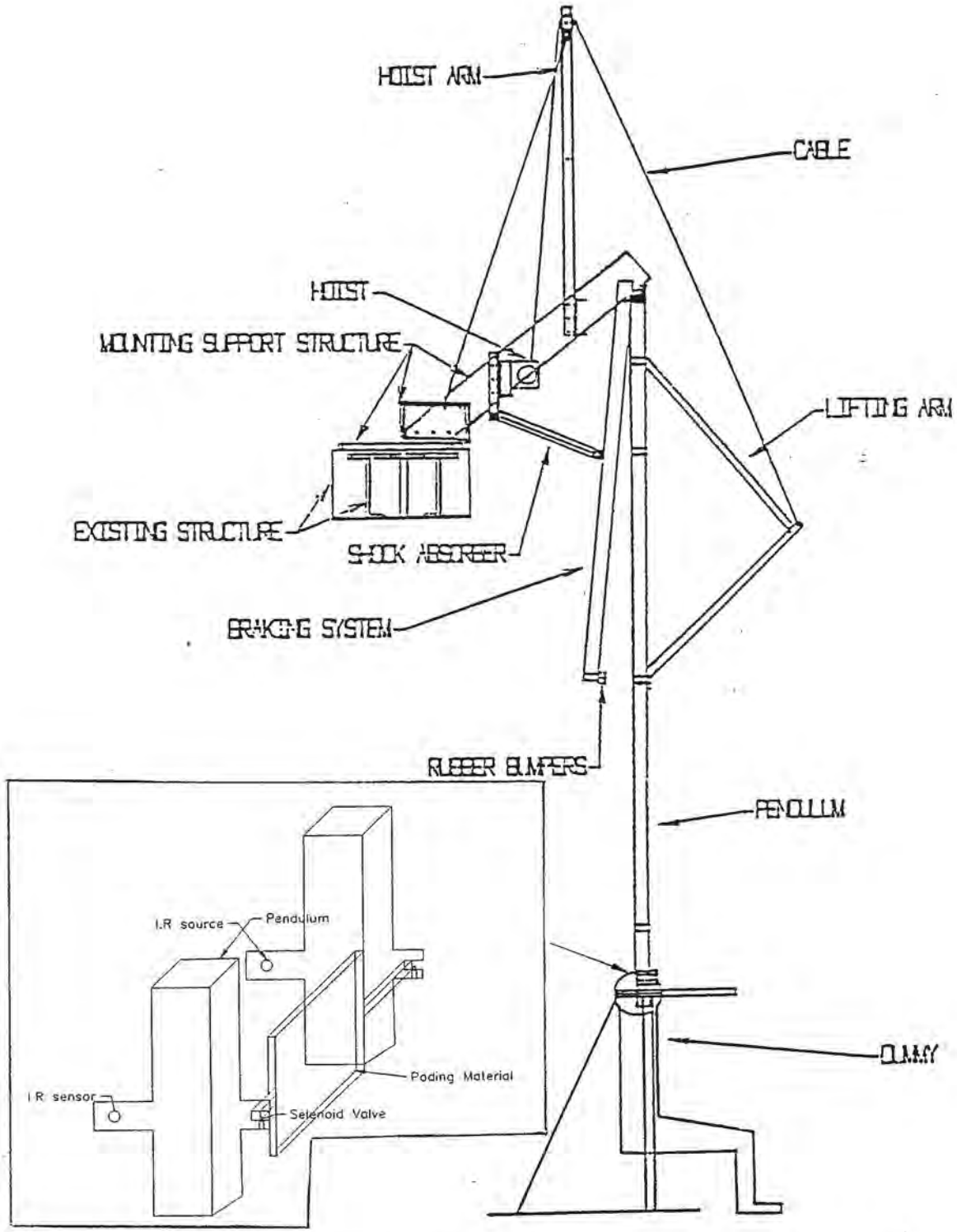

FIGURE 4.3 DETAILS OF PENDULUM TYPE TEST SETUP

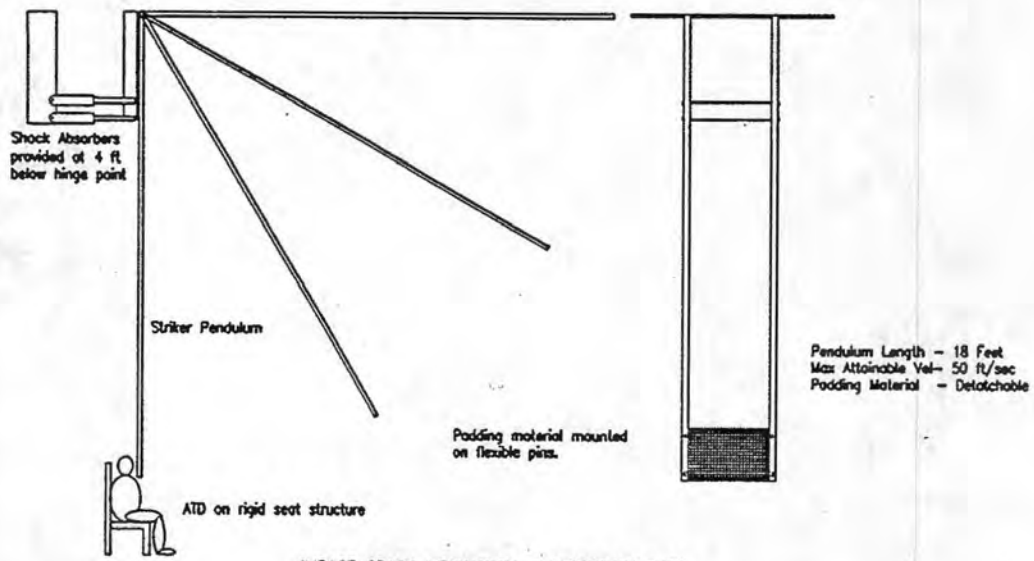

FIGURE 4.4 DETAILS OF PENDULUM TEST SETUP WITH MOUNTING PANEL

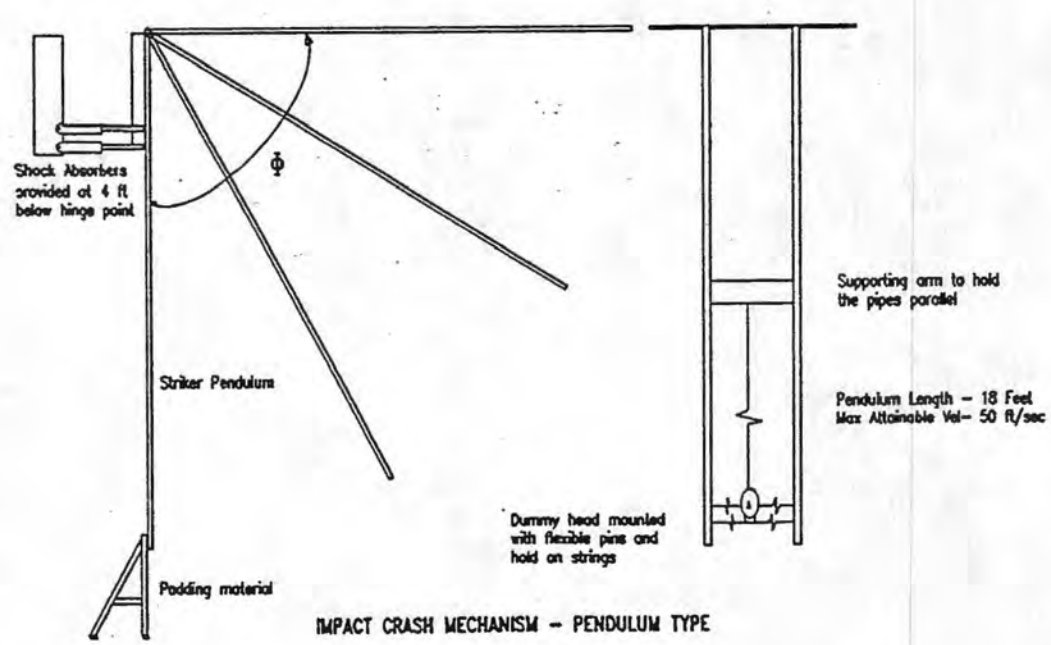

FIGURE 4.5 DETAILS OF PENDULUM TEST SETUP WITH HEAD MOUNTED

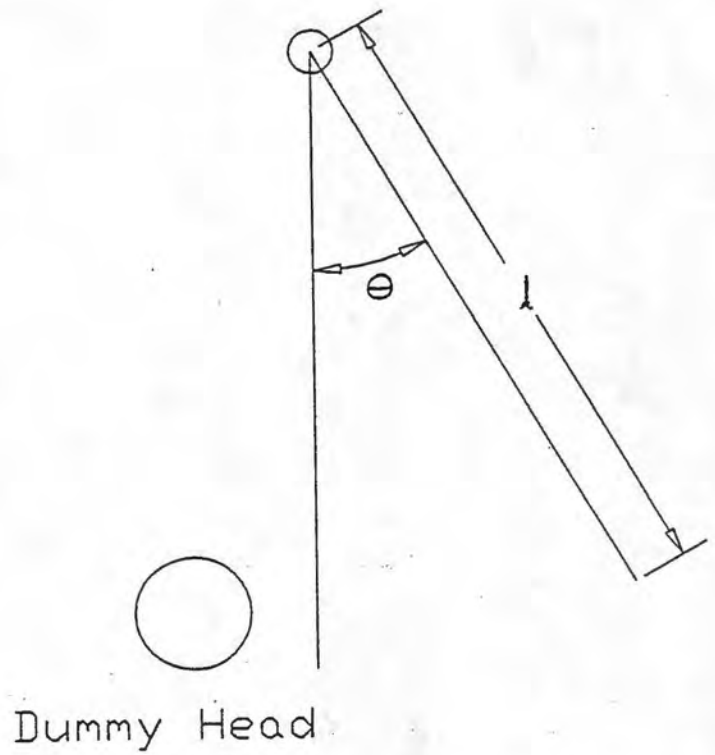

FIGURE 4.6 VELOCITY OF THE HEAD

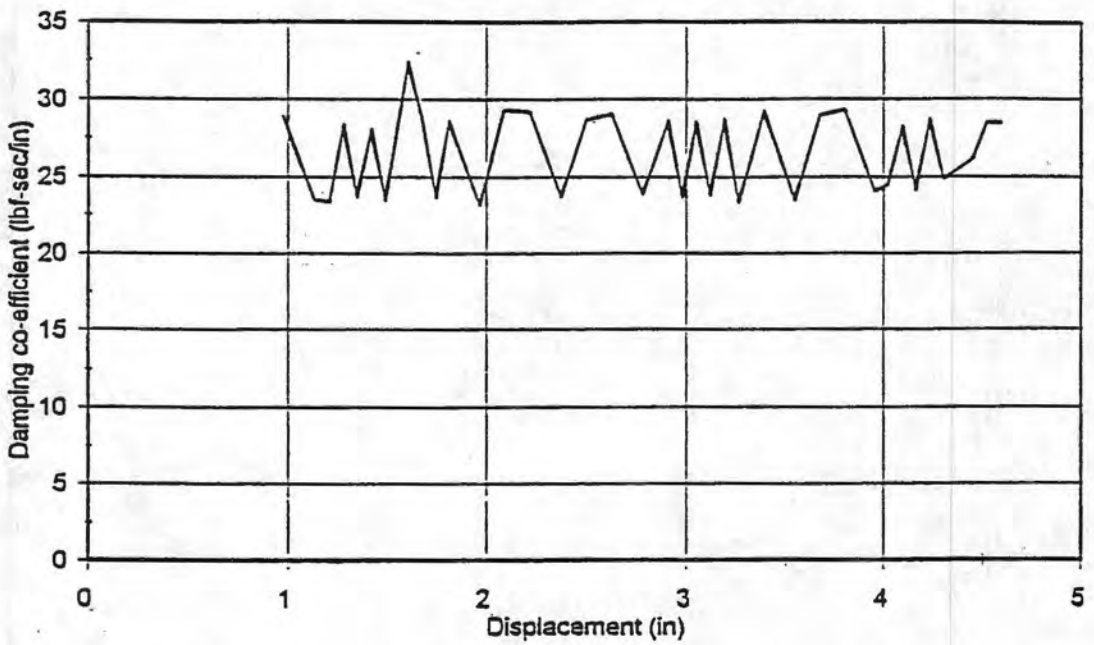

FIGURE 4.7 DAMPING COEFFICIENT RESPONSE AT A DISPLACEMENT RATE OF 1.3 IN/SEC

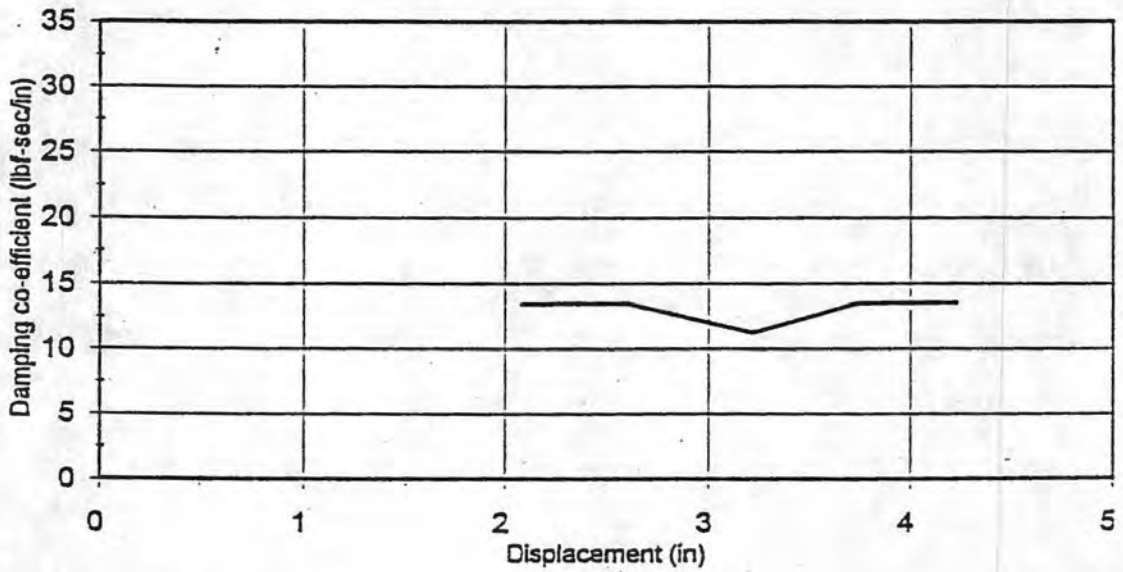

FIGURE 4.8 DAMPING COEFFICIENT RESPONSE AT A DISPLACEMENT RATE OF 4.75 IN/SEC

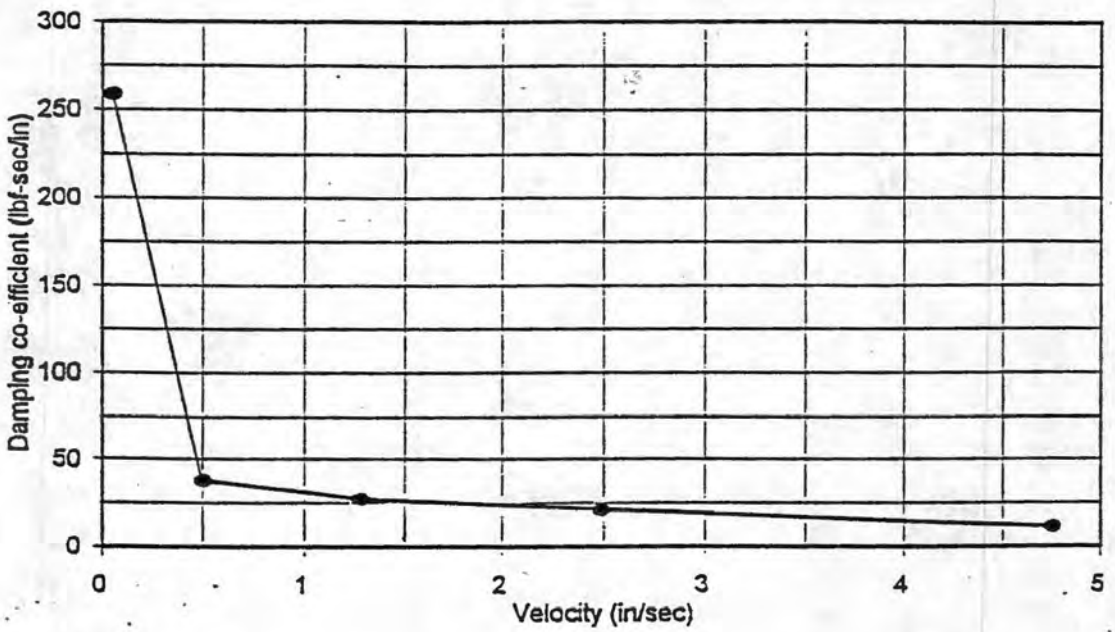

FIGURE 4.9 DAMPING COEFFICIENT AT DIFFERENT VELOCITIES

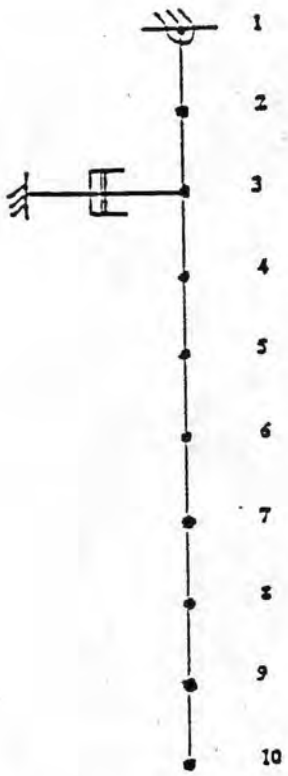

Length of pendulum = 18 ft
Length of element = 2 ft
Number of nodes = 10

FIGURE 4.10 FINITE ELEMENT MODEL OF THE PENDULUM HEAD IMPACT TEST RIG

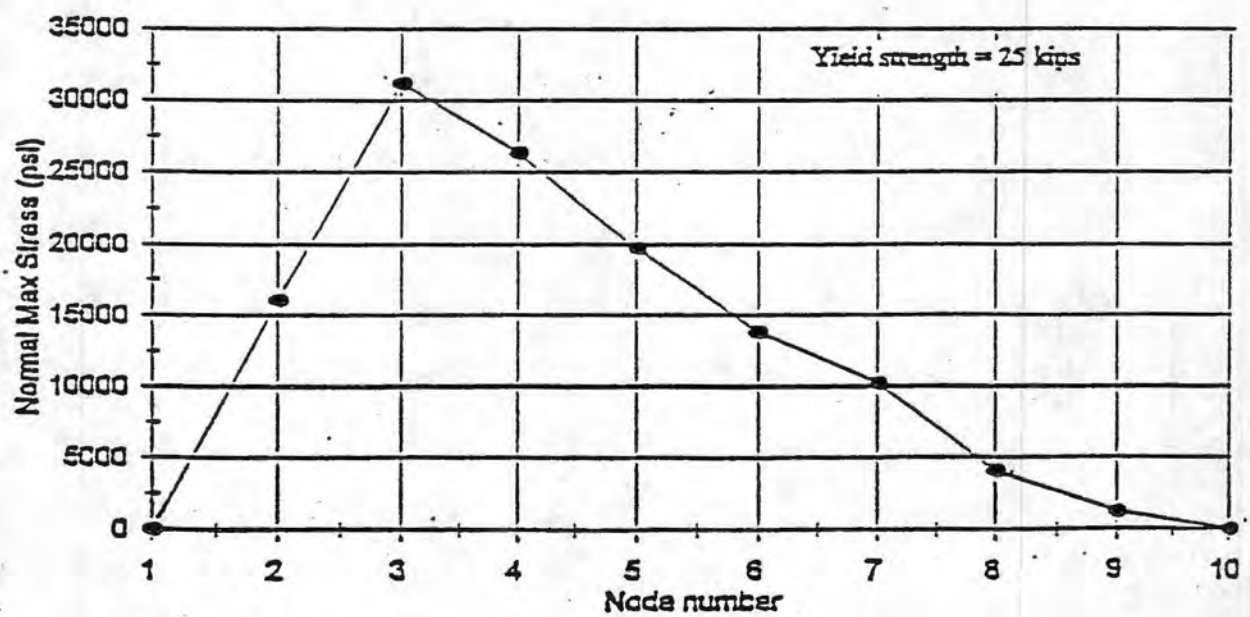

FIGURE 4.11 STRESS DISTRIBUTION FOR 3 IN X 2 IN X 0.25 IN THICK STEEL I SECTION

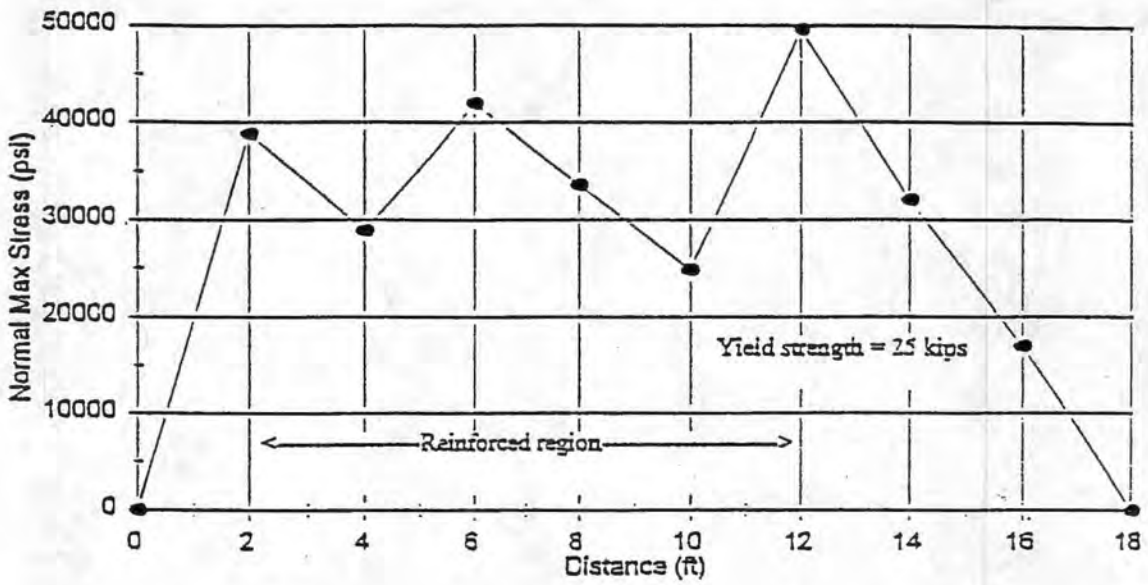

FIGURE 4.12 STRESS DISTRIBUTION FOR 3 IN X 2 IN X 0.25 IN THICK STEEL I SECTION (REINFORCED)

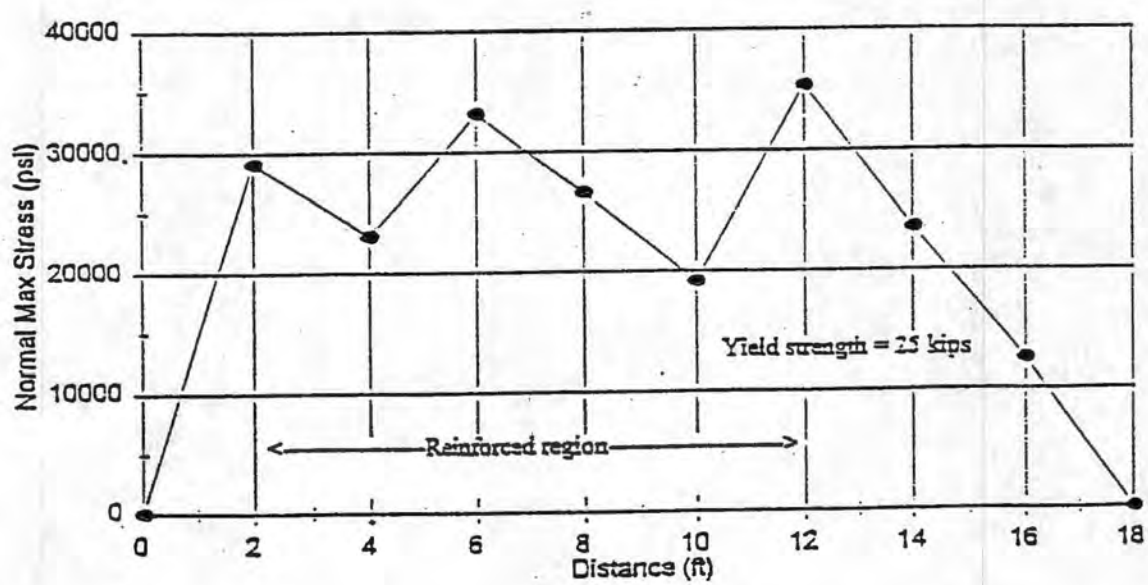

FIGURE 4.13 STRESS DISTRIBUTION FOR 4 IN X 2 IN X 0.25 IN THICK STEEL I SECTION (REINFORCED)

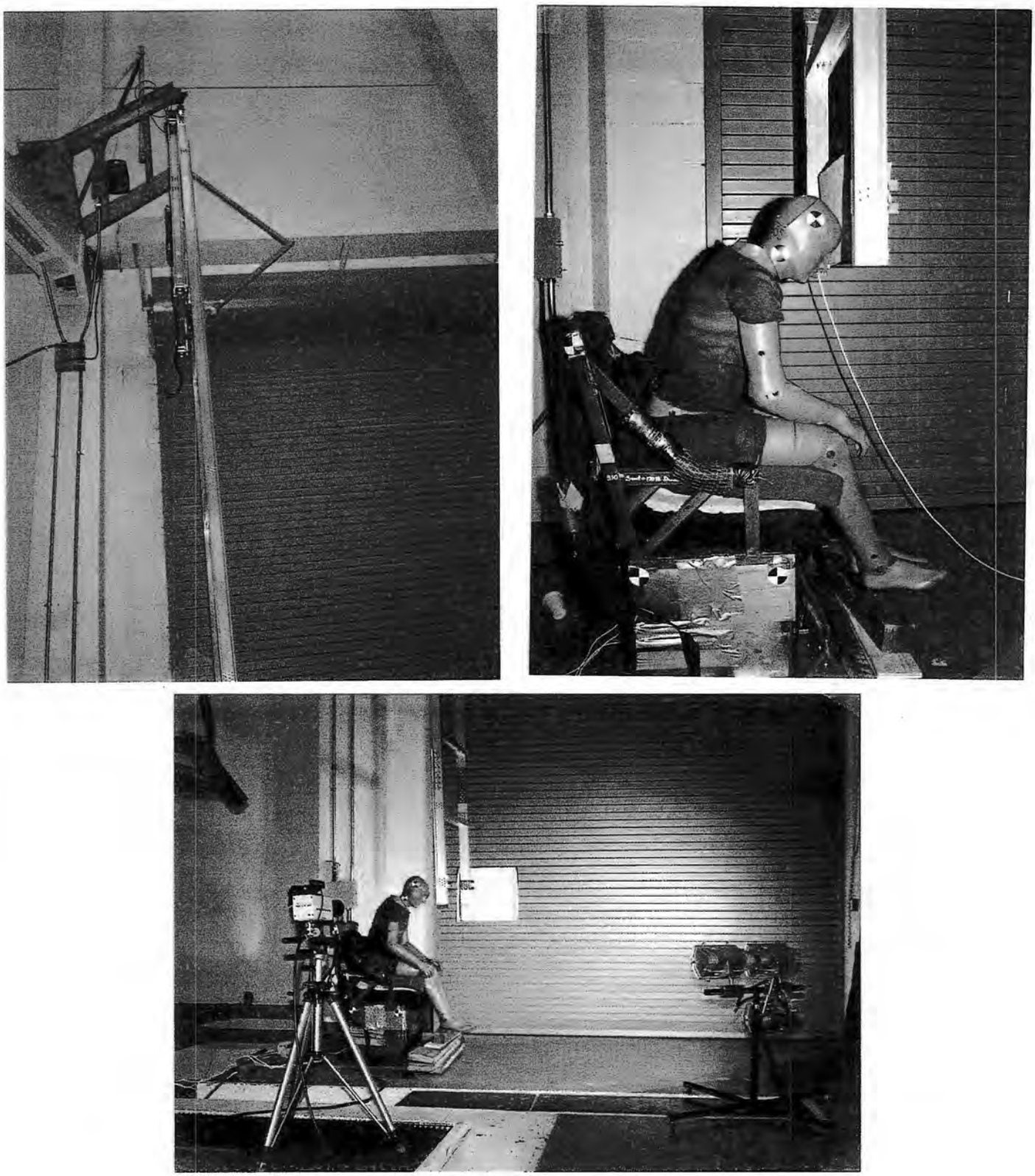

FIGURE 4.14 VIEW OF THE SETUP AT NIAR

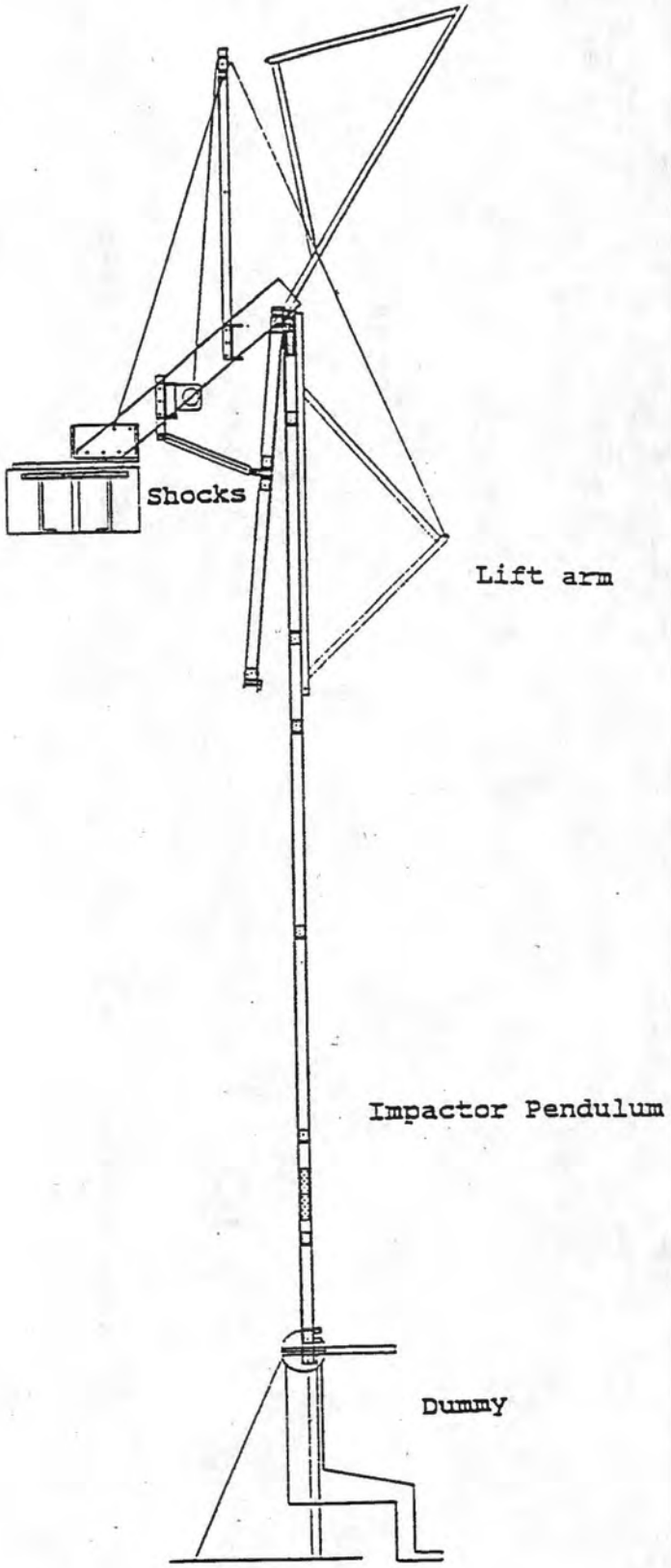

FIGURE 4.15 PENDULUM IMPACT TEST SETUP

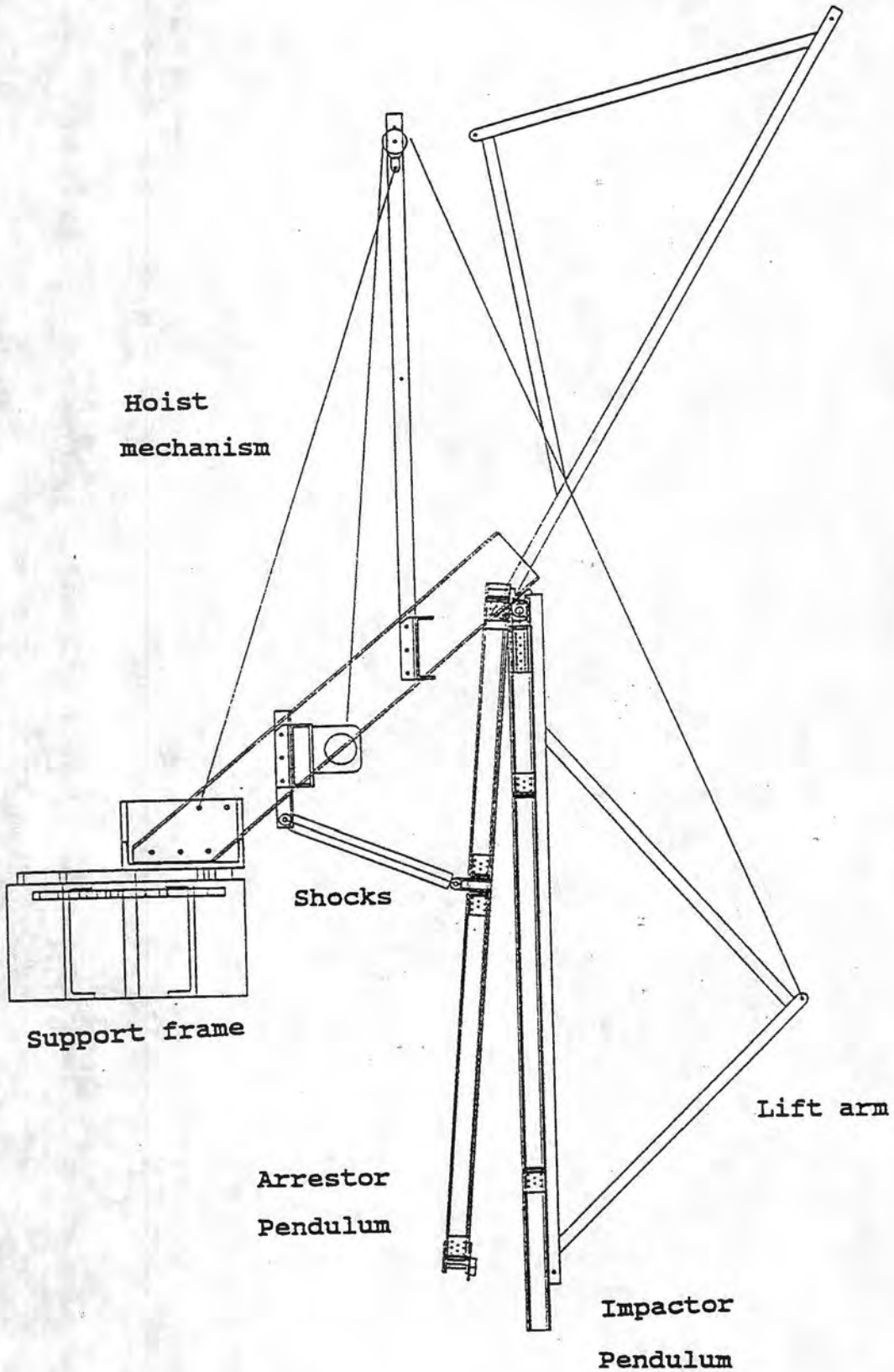

FIGURE 4.16 DETAILS OF THE PENDULUM HOIST ASSEMBLY

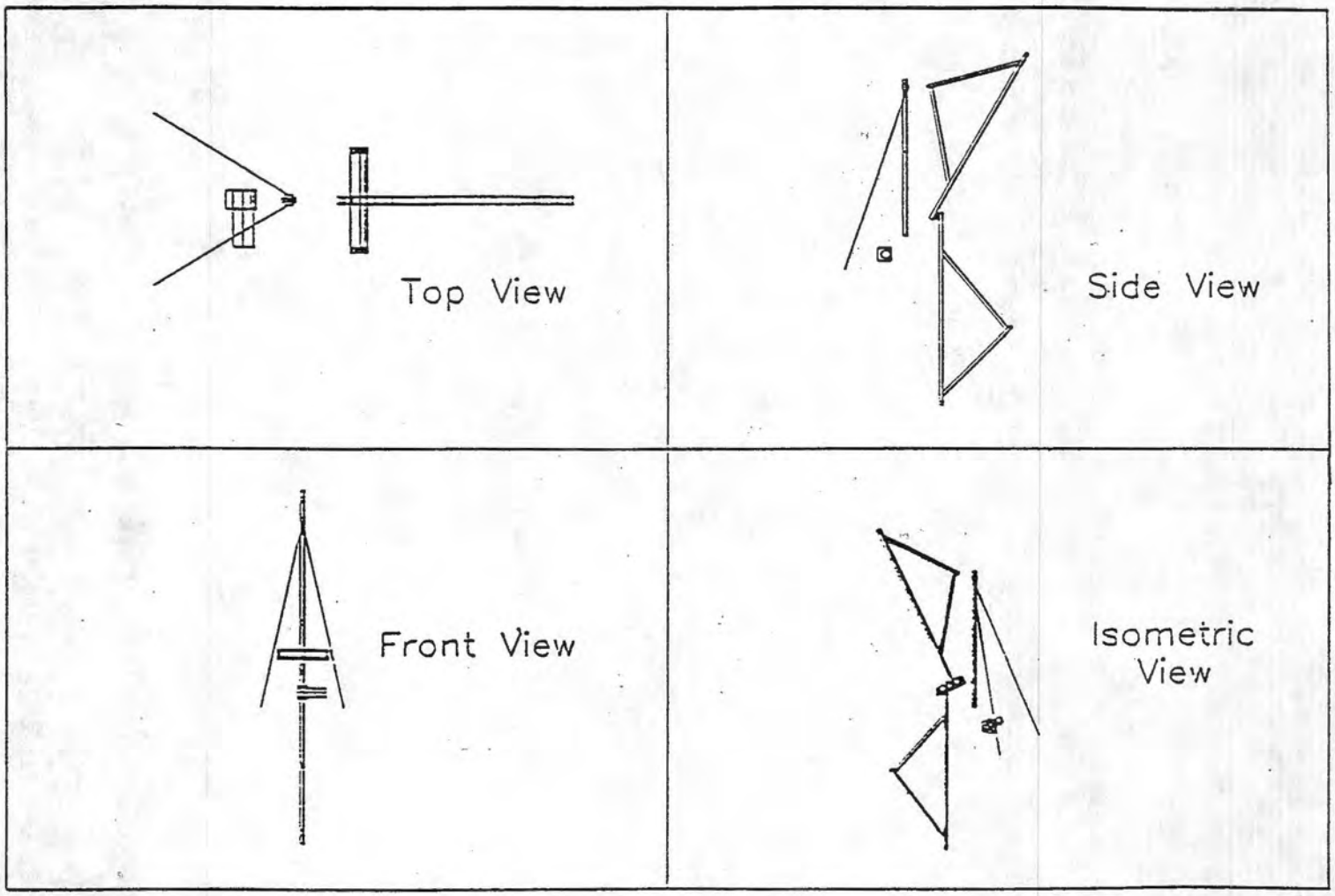

FIGURE 4.17 DETAILS OF THE LIFT ARM

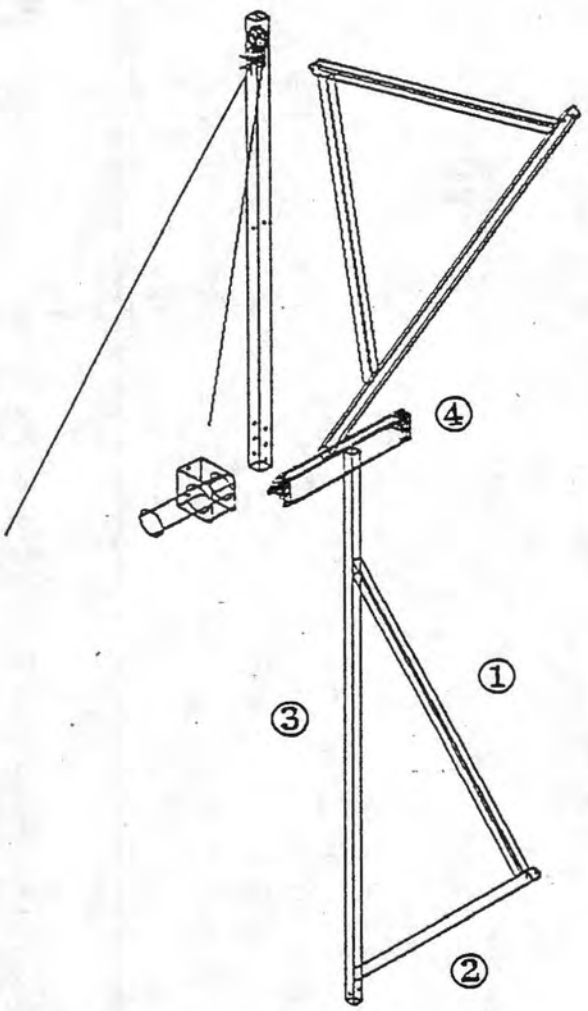

Member	Dimensions
①	3' 11"
②	3' 8"
③	7' 5"
④	1' 10"

FIGURE 4.18 DETAILS OF THE LIFT ARM

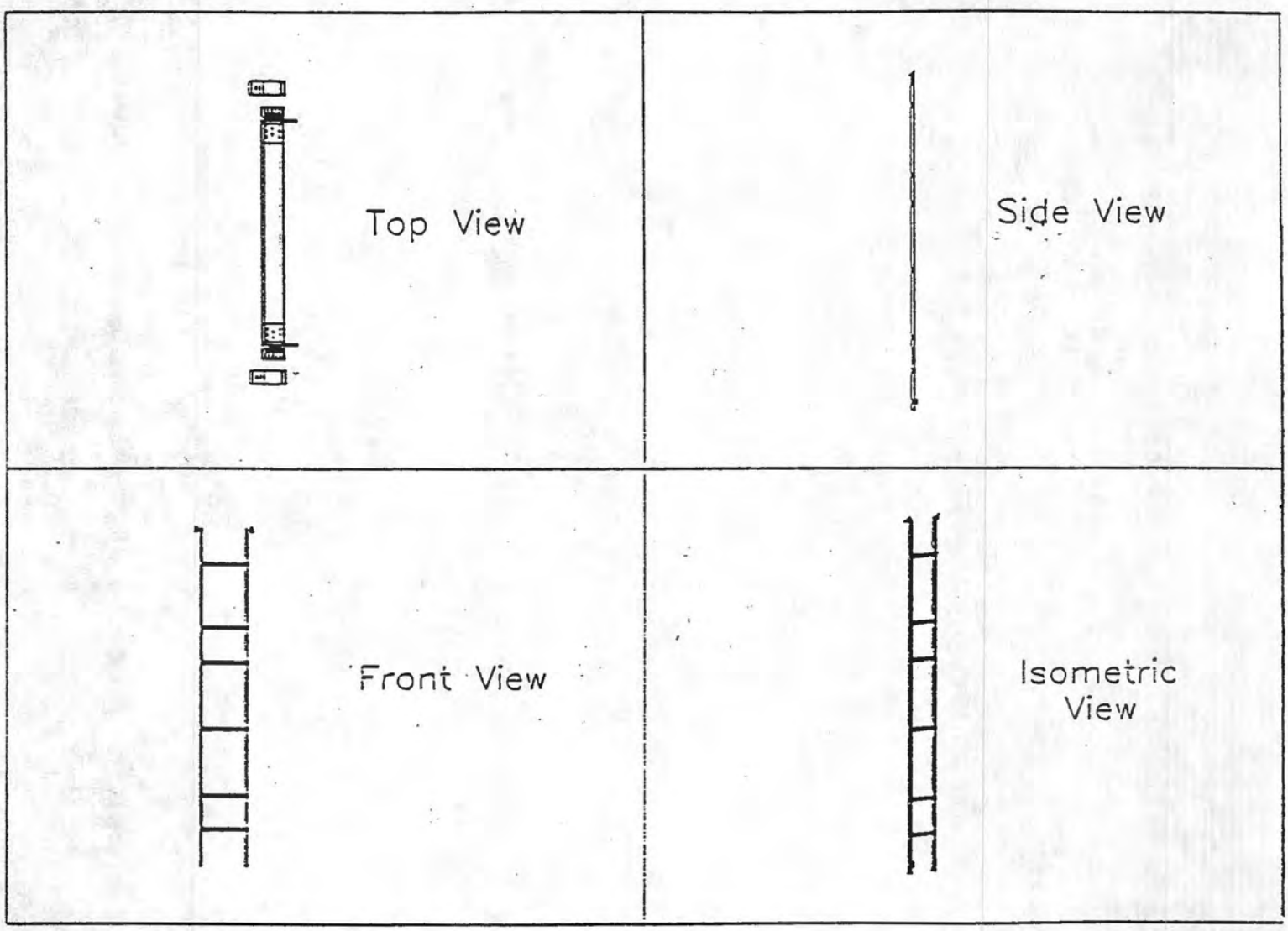

FIGURE 4.19 DETAILS OF THE IMPACTOR PENDULUM

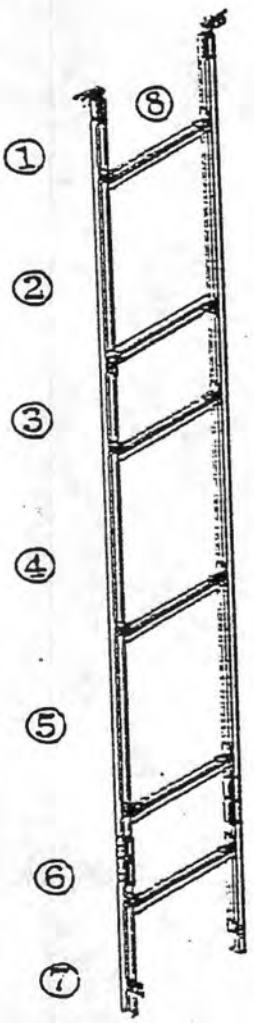

Member	Dimensions
①	2' 1"
②	3' 10"
③	2' 0"
④	4' 0"
⑤	4' 0"
⑥	2' 0"
⑦	1' 1"
⑧	2' 6"

FIGURE 4.20 DETAILS OF THE IMPACTOR PENDULUM

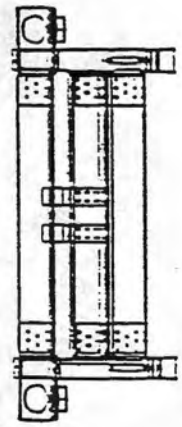

Top View

Side View

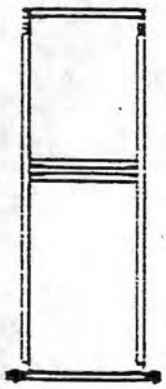

Front View

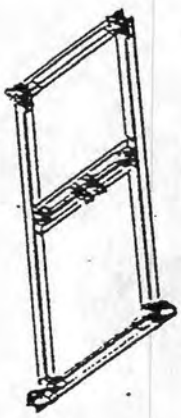

Isometric View

FIGURE 4.21 DETAILS OF THE MOTION ARRESTOR PENDULUM

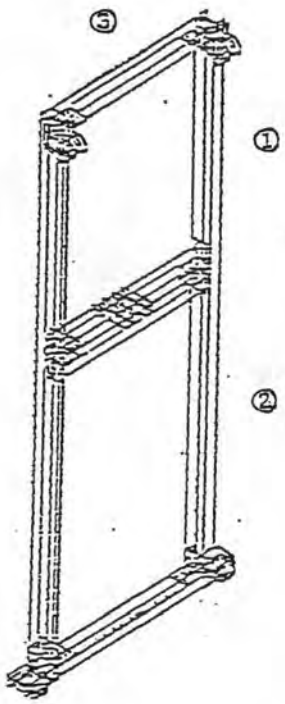

Member	Dimensions
①	3' 0.5"
②	4' 1.5"
③	2' 0.75"

FIGURE 4.22 DETAILS OF THE MOTION ARRESTOR PENDULUM

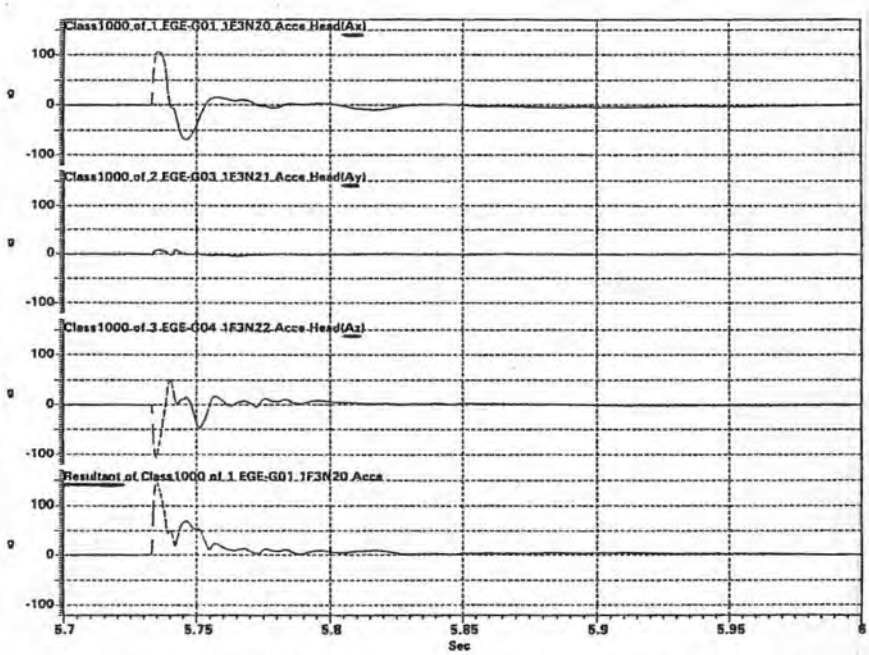

FIGURE 4.23 DECELERATION RESPONSE DURING HEAD IMPACT AT 11.93 FT/S.

5. INJURY CRITERIA FOR NON STANDARD OCCUPANTS

5.1 Introduction

The resultant forces and accelerations that act on a child during a crash scenario is different from that of an adult. But FAR does not specify any injury criteria for a child. Therefore new injury criteria have to be developed in order to validate the child safety systems. Since no child cadaver test results or biomechanical data are available for a child, scaling methods were employed to formulate the child injury criteria. The maximum axial compressive lumbar load for a 3 year old child dummy was formulated by employing the scaling methods. The maximum compressive femur load for a 3 year old child was formulated as discussed below.

5.2 Scaling of the Femur Load

Following assumptions were made in the development of the limiting femur load for a 3 year old child dummy.

a. The femur of the 3 year old child and adult are geometrically similar. Hence the geometric length scale factor (λ_L) is obtained from the relation

$$\frac{\text{Length of Upper Leg of 3 Year Old Dummy}}{\text{Length of Upper Leg of 50th \%ile Hybrid II Dummy}} = \frac{12.7}{20.4} = 0.62$$

The lengths are obtained from reference [1]. Since the femurs are geometrically similar, the area and volume of the 3 year old femur are scaled by λ_L^2 and λ_L^3 respectively.

b. Since the exact geometry of the adult and child femur could not be obtained, the adult and child femur are approximated to have constant cross sectional area. Exact cross sectional dimensions of the adult and child femurs are not needed, since cross sections are approximated by the length scale factor.

c. The stress strain curve for the child femur is similar to that of adult femur [1] as shown Figure (5-1).

From the regression analysis, a correlation between the femur injury load and age was constructed. The Femur Injury Criteria (FIC) equation is given by

$$\text{FIC} = \begin{cases} -116.5 + 116.7 * \text{Age lb} & 3 \le \text{Age} \le 20 \\ 2250 \text{ lb} & 21 \le \text{Age} \le 30 \\ 1690.3 - 6.6 * \text{Age lb} & 31 \le \text{Age} \le 60 \end{cases}$$

5.3 Scaling of lumbar force for child

The physical parameters that influence the fracture of the femur would be a force F, the ultimate stress σ and the cross sectional area A. Since there is no information available about the ultimate properties of the child, difficulty arises in determining the ultimate stress of the child femur. From the available information on the compressive strength of a new born child femur and an adult femur [1], the compressive strength of a 3 year old child was approximated to be 15000 lb/in^2 as seen in Figure (5-2), while the compressive strength of an adult femur was approximately 24500 lb/in^2. Hence the scale factor for the ultimate compressive stress (λ_σ) is

given by

$$\frac{\text{Ultimate Compressive Strength of Child Femur}}{\text{Ultimate Compressive Strength of Adult Femur}} = \frac{15{,}000}{24{,}444} = 0.61$$

Therefore the scale factor for force is obtained from

$$\frac{F_C}{F_A} = \frac{\sigma_C}{\sigma_A} * \frac{A_C}{A_A}$$

$$\lambda_F = \lambda_\sigma * \lambda_L^2$$

$$= 0.61 * 0.62^2$$

$$= 0.24(\text{Approximately})$$

According to the above relationship, the axial compressive fracture load for a 3 year old femur is the product of the fracture load for the adult and the scaling factor. This is found to be approximately 600 lb.

5.4 HIC assessment for three year old child

In an attempt to assess the biodynamic response and injury tolerance for occupants not represented by a Hybrid II ATD, the scaling laws were employed. The analysis was carried out for a 3 year old child dummy. Since the response of a child, in a crash environment is different from that of an adult, it is essential to determine the tolerance limits of children. But FAR does not specify any injury criteria for a child nor any criteria has been developed so far. Hence scaling methods were employed to formulate HIC for a 3 year old child. The maximum axial compressive lumbar load and compressive axial femur load for a 3 year old child was earlier. These again were 300 lb limiting load on the lumbar and 600 lb limiting load on the femur. The following contains formulation of the HIC for a 3 year old child [9].

The origin of HIC lies in the "Wayne State Tolerance Curve," (WSTC) which provided a boundary between a "safe" head response and an "unsafe" head response [2-4]. The data of the WSTC were obtained from experiments on dogs by measuring the intracranial pressure and from cadaver tests [5]. The curve was originally a plot of "effective head acceleration" versus time duration. It was claimed, that the dividing line represents the onset of brain concussion in Figure (5.1). WSTC was based on the hypothesis that the dominant head injury mechanism is linear acceleration. Therefore any attempt to scale the HIC for a 3 year old child should start from WSTC. When the WSTC curve of an adult is drawn on a log-log plot, it takes the form of an approximate straight line as seen in Figure (5.2). The equation of this straight line is given by

$$A\, t^{0.4} = 15.83 \qquad (5.1)$$

With suitable multiplication, Equation (5.1) can be changed to

$$A^{2.5}\, t = 1000 \tag{5.2}$$

where 't' is the duration of constant acceleration A and 1000 is the tolerance limit. This equation was known as Gadd Severity Index (GSI) represented in Figure (5.3)[6]. GSI was further modified by replacing the constant acceleration with an effective acceleration and was represented by

$$GSI = \int_{t_1}^{t_2} [A(t)]^{2.5}\, dt = 1000 \tag{5.3}$$

where, A(t) is the effective head acceleration as a function of time and the integral is over the entire pulse duration.

GSI was subsequently replaced by HIC, which is defined as

$$HIC = \left[\frac{1}{t_2 - t_1} \int_{t_1}^{t_2} A\ dt\right]^{2.5}_{max} (t_2 - t_1) = 1000 \tag{5.4}$$

where, again A(t) is the resultant linear acceleration at the center of gravity of head and t_2 and t_1 are arbitrary instant of time when head experiences acceleration or deceleration. The size of window (t_2-t_1) has been fixed as 36 ms [7].

The translational acceleration limits for children can be determined from the critical values of adults by the use of mechanics of similitude. According to Sturtz [8], the concussive level of brain, due to translational acceleration, for children can be estimated from,

$$A_c = A_a \left[\frac{M_a}{M_c}\right]^{\frac{1}{3}} \tag{5.5}$$

where

A_c - Translational acceleration limit of child.

A_a - Translational acceleration limit of adult.

M_a - Mass of adult brain.

M_c - Mass of child brain.

The mass of a 3 year old brain has been determined as 1.09 kg. and that of an adult varies from 1.29 to 1.43 kg.[8]. If the average brain mass of an adult is taken as 1.36 kg., then the limiting translational acceleration for a 3 year old child is

$$A_c = 1.077\ A_a \tag{5.6}$$

Equation (5.6) can then be used to approximate the WSTC for a 3 year old child . The WSTC, for a child, when drawn on a log-log plot can be represented by

$$A\ t^{0.403} = 16.88 \tag{5.7}$$

With suitable multiplications Equation (5.7) can be approximated to

$$A^{2.5}\, t = 1200 \tag{5.8}$$

Hence the GSI for a 3 year old child takes the form

$$GSI = \int_{t_1}^{t_2} [A(t)]^{2.5}\, dt = 1200 \tag{5.9}$$

and HIC takes the form

$$HIC = \left[\frac{1}{t_2 - t_1} \int_{t_1}^{t_2} A\, dt\right]_{max}^{2.5} (t_2 - t_1) = 1200 \tag{5.10}$$

This equation states that when analysis or sled test experiments are performed for a 3-year old child dummy, in order to assess the amount of possible head injury, the variable HIC is evaluated as before; however, the threshold of injury would be 1200 for child. This result needs to be tested for a number of test cases in order to gain confidence in the use of equation (5.10).

5.5 References

1. Yamada, H., "Strength of Biological Materials," Edited by Evans, F.G., The Williams & Wilkins Company, Maryland, 1970.

2. Gurdjian, E.S., Lissner, H.R., Latimer, F.R., Haddad, B.F., Webster, J.E., "Quantitative Determination of Acceleration and Intracranial pressure in Experimental Head Injury," Neurology, Vol 3, June 1953, pp 417-423.

3. Gurdjian, E.S., Roberts, V.L., Thomas, L.M.,"Tolerance curves of Acceleration and Intracranial Pressure and Protective Index in Experimental Head Injury," J.Trauma, pg 600, 1964.

4. Gurdjian, E.S., Hodgson, V.R., Hardy, W.G., Patrick, L.M., Lissner, H.R., "Evaluation of the Protective Characteristics of Helmets in Sports," J.Trauma, Vol 4, 1964.

5. Lankarani, H.M., Malapati, S.R., Menon, R., "Evaluation of Head Injury Criteria," NIAR Report 93-2, 1993.

6. Gadd, C.W., "Use of a Weighted-Impulse Criterion for Estimating Injury Hazard," SAE Paper No. 660793, Proceedings of the Tenth Stapp Car Crash Conference, Nov. 1066.

7. "MADYMO User's Manual 2-D," Version 5.0, 1992.

8. Sturtz, G., "Biomechanical Data of children," Paper No. 801313, Proceedings of the Twenty-fourth Stapp Car Crash Conference, pp 511-559. Williams and Willkins Company, Baltimore, 1970.

9. Periannan, K., "Evaluation of Occupant Dynamic Responses and Development of Injury Criteria for a 3 year old Child," M.S. Thesis, Wichita State Univrsity.

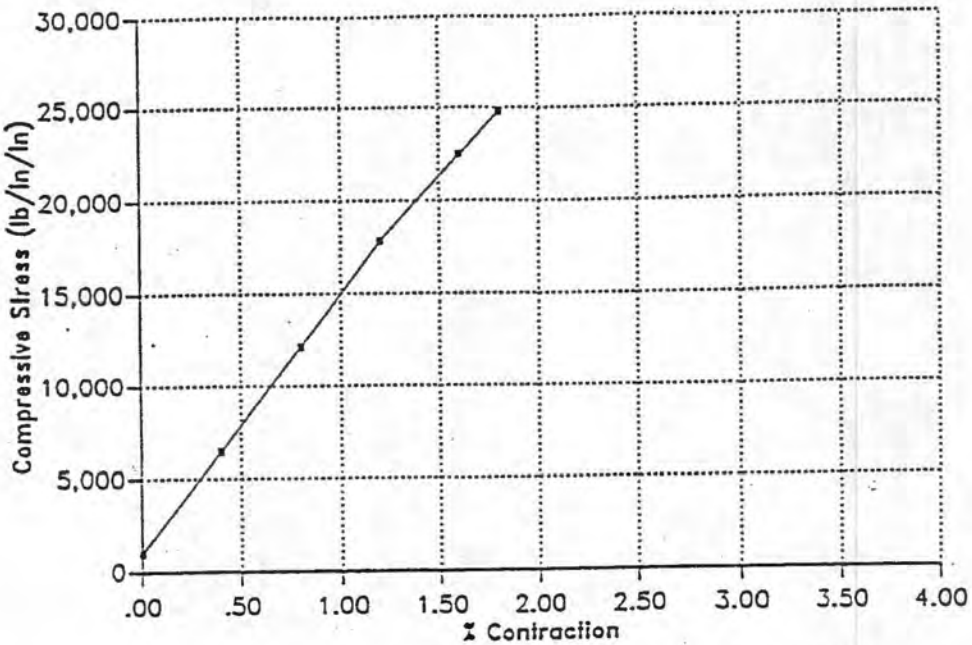

FIGURE 5.1 STRESS STRAIN CURVE OF ADULT FEMUR

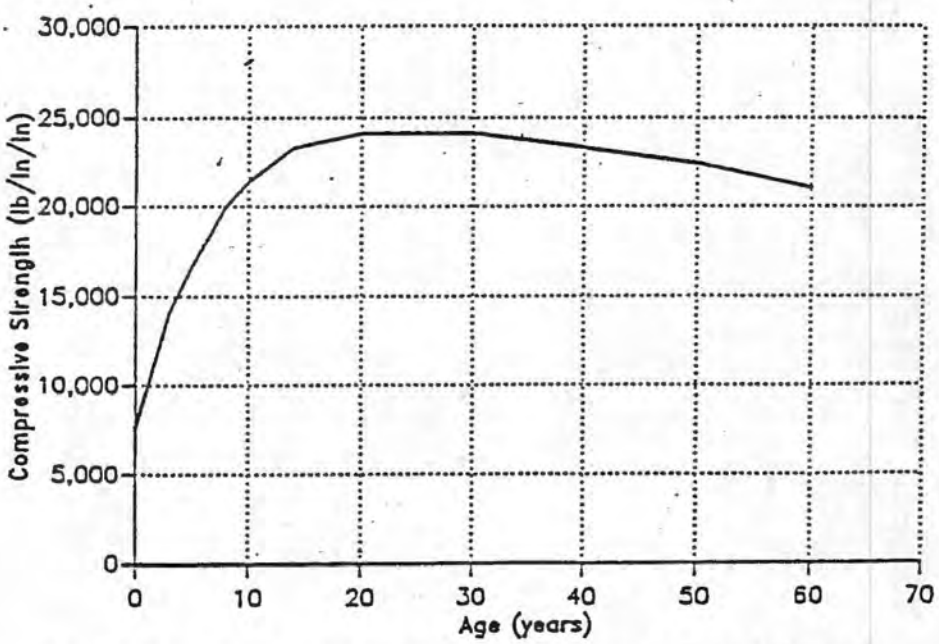

FIGURE 5.2 ULTIMATE COMPRESSIVE STRESS VS AGE

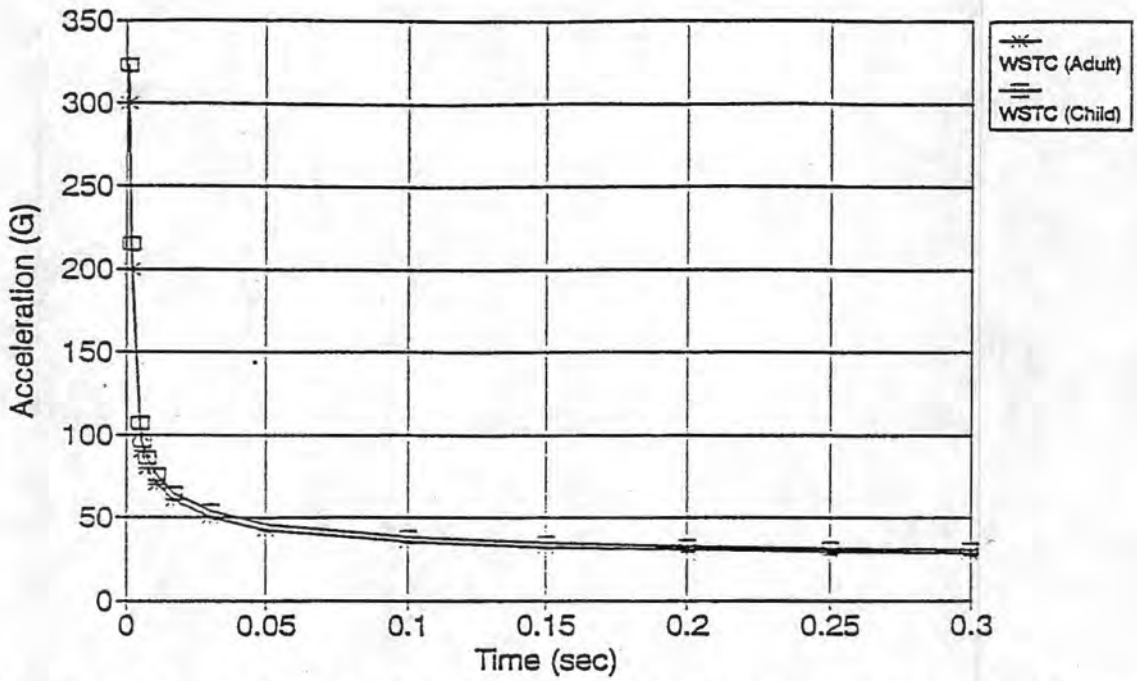

FIGURE 5.3 WAYNE STATE TOLERANCE CURVE FOR ADULT AND CHILD

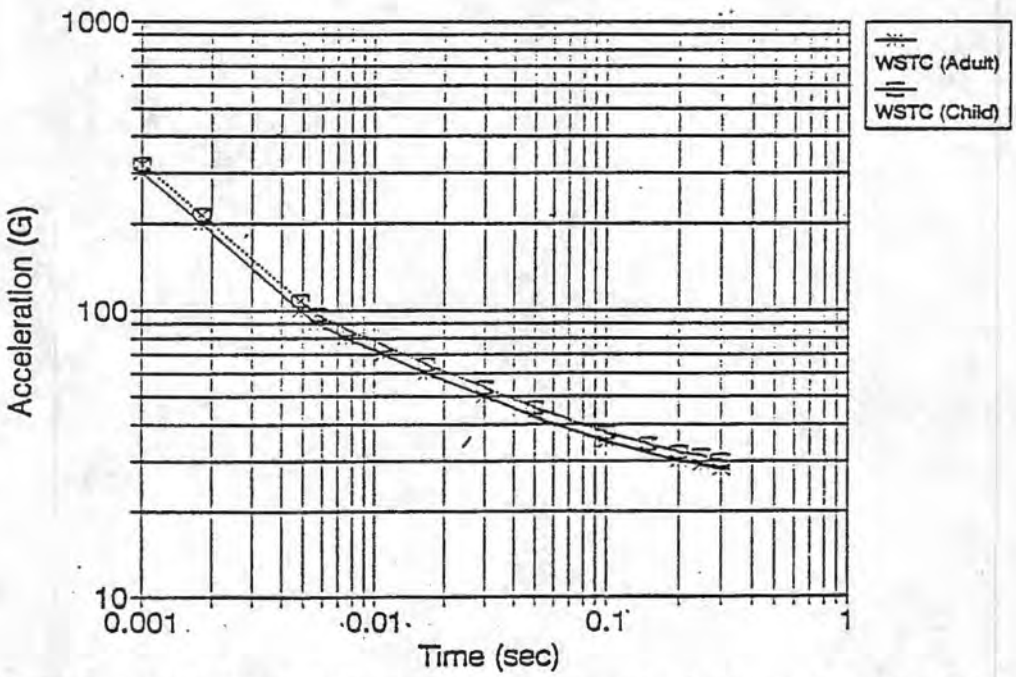

FIGURE 5.4 WAYNE STATE TOLERANCE CURVE FOR ADULT AND CHILD ON A LOG-LOG SCALE

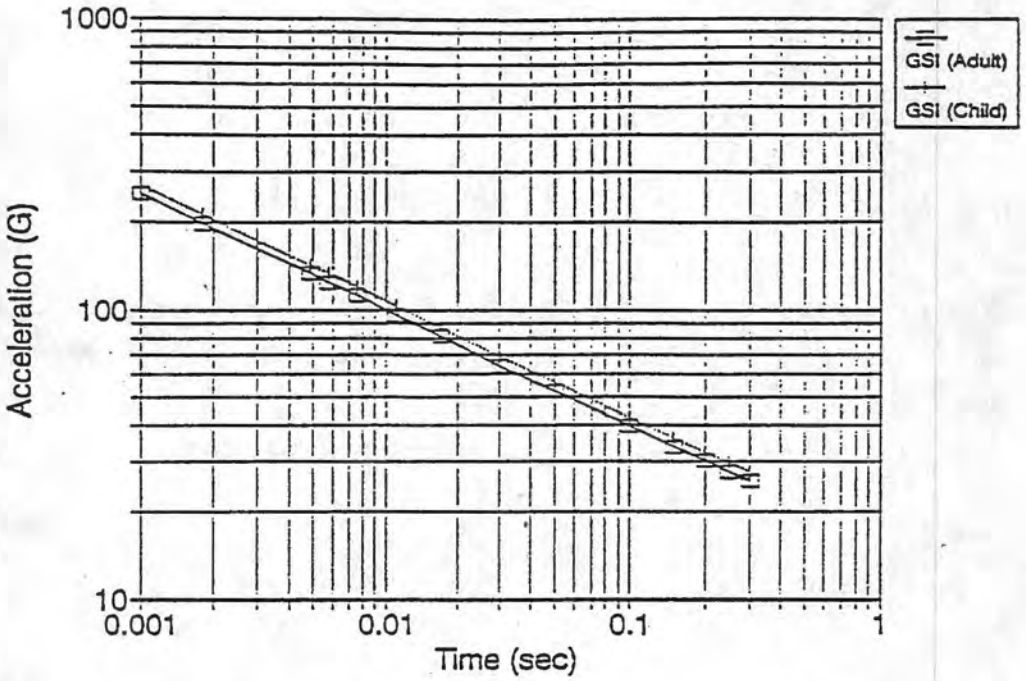

FIGURE 5.5. GADD SEVERITY INDEX FOR ADULT AND CHILD

6. CHILD SEAT/RESTRAINT SYSTEM

6.1 Introduction

In an effort to improve the crash survivability of children, a study was performed using the code 'MADYMO' to identify the criteria for the design and development of seat and restraint systems [1,2]. An integrated seat as shown in Figure (6.1) was designed for this purpose and three different tests were simulated for the performance evaluation of 3 year old child dummy. In the first impact test, a frontal impact was simulated to assess the restraint strength and also to measure the amount of head excursion allowed by the shoulder harness. In the second test, oblique impact was simulated by aligning the seat at 10 degree yaw. In the third impact test, vertical impact was simulated by aligning the seat at 60 degree pitch to measure the compressive forces acting on the lumbar region.

6.2 Frontal impact simulation test

In this test, a 16 g triangular pulse requiring a time interval of 0.09 seconds to reach the peak was applied to the seat. Five different types of restraint systems were employed to determine their effectiveness in holding the child occupant in frontal impact. The effect of using two point restraint system (lap belt) and 5 point harness system (shoulder belt) on the HIC value, head excursion, resultant peak accelerations of pelvis, chest, head were studied. It was found that the five point harness system is effective compared to the two point harness system. The restraints tested were designed to restrict their use to latched or fixed-back seat. The results of the analysis are shown in Table (6.1) and (6.2).

6.3 Oblique impact test

A 10-degree yaw test was conducted for the child dummy to simulate an oblique impact which may occur during an aircraft crash. Only five point restraint system with Nylon XXVIII was analyzed. The result is shown in Table (6.3).

6.4 Vertical impact test

Third test was vertical impact test simulated by aligning the seat at 60 degree pitch to measure the compressive forces acting on the lumbar region. The pulse applied was a 14g triangular pulse requiring a time of 0.08 seconds to reach the peak. In performing this test, the dummy was modelled as a rigid structure. Three different types of cushions viz. baseline, rigid, soft were used to determine the effect of their stiffness on the occupant. The peak results of all the test are tabulated in Table (6.4).

6.5 Conclusions

From the analyses conducted, the following conclusions were drawn.

i. When two point restraint system (lap belt) was used, the HIC values extended well over proposed limit of 1000. This fact can be attributed to the impact of the child head with its lower legs in this restraint configuration. The head accelerations were very high and were in the range 200 to 202 g's. The head excursions were high and were about 15 inches.

ii. In the five point harness (shoulder belt) test without yaw, the HIC values were in the safe limits. The pelvis, chest and head did not experience very high accelerations and were in the safe limits. The head excursions were reduced to 25 % of the lap belt only test.

iii. In the five point harness system test with 10 degrees yaw, no appreciable difference was observed in the performance of the child dummy compared to the five point harness system test without yaw. However, a continuous movement of head and legs in lateral direction were observed but, the dummy was retained with in the seat.

iv. For vertical impact test, the peak values observed with rigid cushion are less when compared to the values obtained with baseline and soft cushions. With soft cushion, the lumbar load observed was 377 lb., which is well above the proposed limit of 300 lb [1], scaled from the limiting load for adults. However, with the other two cushions, the lumbar loads were below the proposed limit.

From the above conclusions, it can be stated that a child seat with a 5 point restraint system and with either baseline or rigid cushion will provide effective crash protection for a child.

6.6 References

1. Perianan K., "Evaluation of Occupant Dynamic Responses and Development of Injury Criteria for a 3 Year Old Child," M.S. Thesis, Wichita State University, 1994.

2. Kompalli C., "Design of Integrated Child Restraint System for Aircraft Crash Protection," M.S. Thesis, Wichita State University, 1994.

TABLE 6.1- PEAK VALUES FOR HORIZONTAL TEST WITH ONLY LAP BELT

Restraint	Type	Peak Resultant Acceleration (g)			HIC	Head Excursion(in)	Head-Neck Angle (deg)	Lap Belt Load (lb)
		Pelvis	Chest	Head				
Polyester	Lap belt	20.0	54.0	202	2504	15.2	37.0	1119
Nylon VII	Lap belt	19.8	52.3	201	2552	15.5	37.0	1101
Nylon IX	Lap belt	20.2	52.0	201	2541	15.3	36.7	1098
Nylon XXVIII	Lap belt	19.4	50.7	202	2584	15.6	36.5	1097
Nylon FTMS	Lap belt	20.5	51.4	200	2579	15.7	37.2	1067

TABLE 6.2 - PEAK VALUES FOR HORIZONTAL TEST WITH SHOULDER HARNESS

Restraint	Type	Peak Resultant Acceleration(g)			HIC	Head Excursion (in)	Head-Neck Angle (deg)	Shoulder Harness Load (lb)
		Pelvis	Chest	Head				
Polyester	5 Point	19.6	24.3	35.7	108	4.40	44.7	1137
Nylon VII	5 point	19.3	24.0	37.0	126	4.60	45.1	987
Nylon IX	5 Point	19.3	23.1	37.1	121	4.60	45.0	1020
Nylon XXVIII	5 Point	19.1	22.3	36.0	138	4.65	45.0	901
Nylon FTMS	5 Point	20.7	23.9	36.2	150	4.88	45.2	924

TABLE 6.3 - PEAK VALUES FOR 10^0 YAW TEST

Restraint	Type	Peak Resultant Acceleration (g)			HIC	Head Excursion (in)	Shoulder Harness Load(lb)		
		Pelvis	Chest	Head			Left	Right	Total
Nylon XXVIII	5 Point	27.4	21.3	30.0	118	4.6	453	499	952

TABLE 6.4 - PEAK VALUES FOR VERTICAL TEST

Cushion	Belt Type	Peak Resultant Acceleration (g)			HIC	Lumbar load (lb)
		Pelvis	Chest	Head		
Baseline	5 Point	18.2	15.1	21.9	34	272
Rigid	5 Point	16.4	16.5	16.3	23	217
Soft	5 Point	27.4	19.0	34.1	75	377

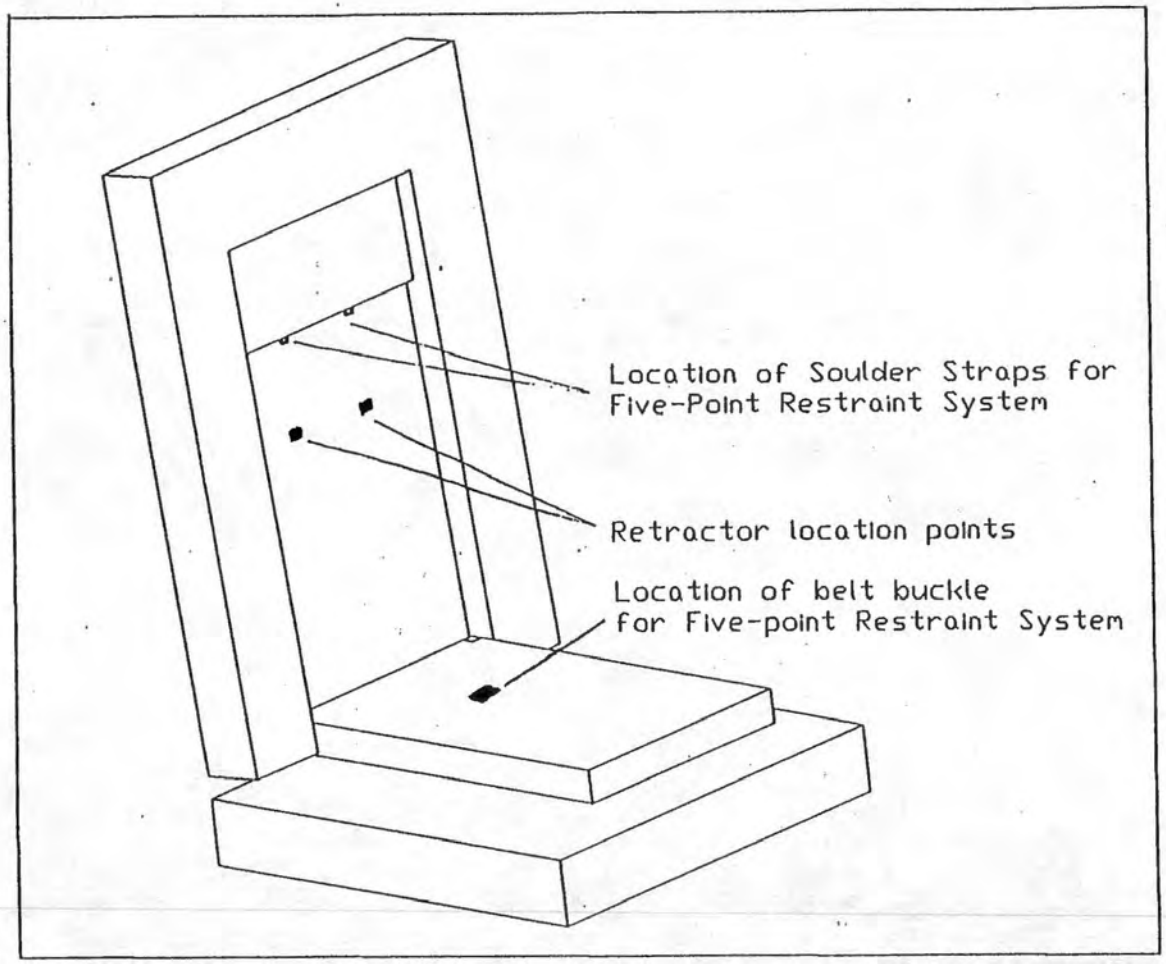

FIGURE 6.1 INTEGRATED CHILD SEAT

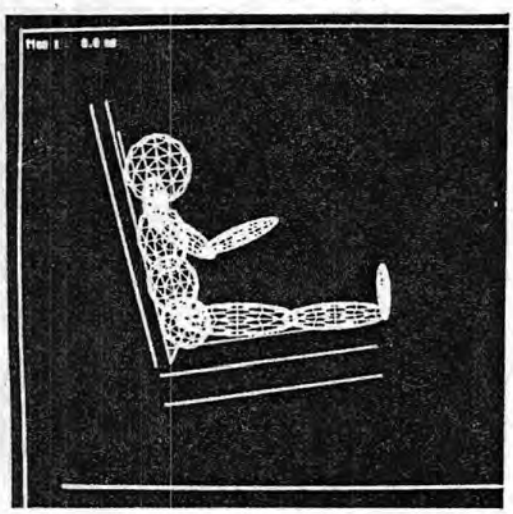

Time: 0.0 ms

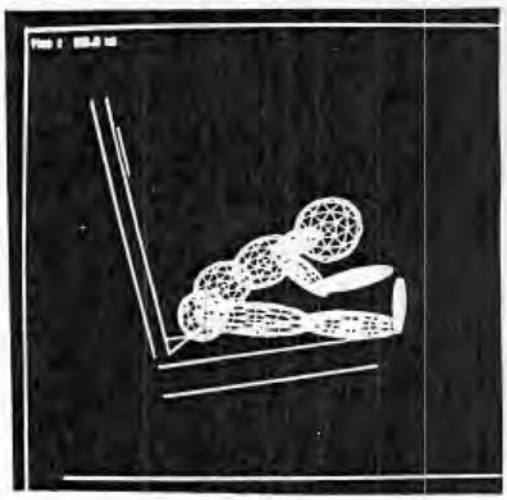

Time: 120.0 ms

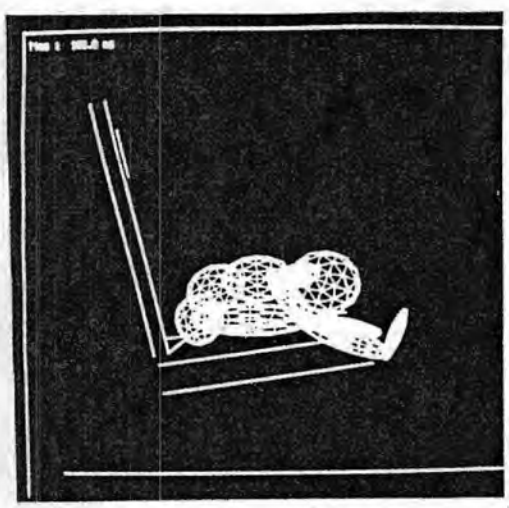

Time 160 ms

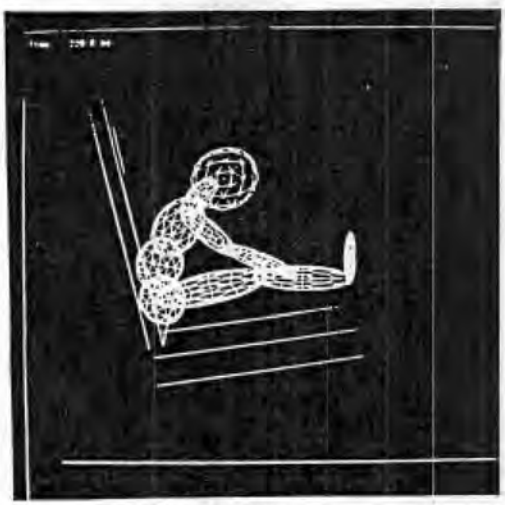

Time: 220 ms

FIGURE 6.2 SIMULATION OF CHILD RESPONSE AT 16 G'S FRONTAL IMPACT

7. ANALYSIS OF SEAT STRUCTURE USING PLASTIC HINGE THEORY

7.1 Introduction

The knowledge of structural responses of an aircraft seat will help in understanding and determining one of the causes of injuries that may be sustained by occupants during a crash. One of the structures which is of immediate concern is a seat structure. A mathematical model of an aviation seat structure has been developed based on plastic hinge modeling approach. The plastic hinge model approach is selected due to its simplicity compared to a finite element model. The plastic hinge modeling and analysis of some elementary structures and the aviation seat structure were carried out [1]. Also, rigid-flexible multibody analysis was carried out for the seat structure.

7.2 Analysis of Cantilever and L-Frame

Before actually applying the plastic hinge modeling to complicated structures, its effectiveness and simplicity can be demonstrated by predicting the behavior of some elementary structures. The collapse mechanism and the amount of plastic deformation incurred in a structure can be readily predicted when the moment-angle diagrams are studied. When a structure is worked beyond the yield point, the total hinge rotation is made of two parts i.e., the hinge rotation in elastic portion and hinge rotation in plastic portion. The hinge rotation in elastic rotation is recoverable and the rotations of the plastic portion are not, subjecting the structure or hinge to permanent deformation. Thus, it is possible to predict the amount of retained deflection in a structure, given the nature of load which would plastically deform the structure. The plastic hinge model of a cantilever beam consists of a torsional spring and a revolute joint at its fixed end as shown in Figure (7.1). Similarly, the plastic hinge model of the L-frame consists of two torsional springs and two revolute joints. The rotations of these plastic hinges directly correspond to the deflection of the members or links attached to the hinges. The dynamic analysis of the system was carried out using the Dynamic Analysis Program [2]. The force at the tip of the rigid member is simulated by a force and a moment at the center of the rigid member. Figures (7.2) and (7.3) demonstrate the behavior of some simple structures like cantilever beam and L-frame. Figure (7.4) shows the moment-angle diagram for a cantilever beam loaded at the tip for a brief amount of time and removed. The load is high enough to deform the structure beyond the yield point. Figure (7.5) and (7.6) shows the moment-angle diagram for an L-frame. It can be observed that two hinges retain different amount of permanent rotation. Figure (7.7) shows the pictorial illustrations of behavior of a torque box representing a passenger compartment using the plastic hinge modeling.

7.3 Analysis of Aviation Seat Structure

The plastic hinge model and response of an Aviation seat are shown in Figure (7.8), (7.9), (7.10). This has five plastic hinges and five rigid links. The load was applied in between hinges 3 and 4 and was analyzed with Dynamic Analysis Program. To simplify the analysis, an equivalent joint rotational stiffness at the joints was used. The equivalent stiffness of the

system is the effective stiffness of the five stiffness in series. This is distributed equally at the five joints. This has the advantage of describing only one history parameter for the stiffness.

7.4 Validation of Plastic Hinge Model

To validate the plastic hinge analysis, the results were compared with finite element results. A linear static analysis of the seat was carried out using the code COSMOS/M. The 2-D finite element model with beam elements is shown in Figure (7.11). All the nodes were constrained to rotate about the X and Y axes. Also, the displacement in the Z direction was constrained. The load was applied at node 20 (Figure 7.11). The results obtained are shown in Table (7.1). They are in good agreement.

7.5 Nonlinear Static Finite Element Analysis

Nonlinear behavior of the aircraft seat structure was accounted in the form of material nonlinearity and analyzed using the code COSMOS/M. Huber-von Mises model was used for describing the material parameter in the form of a bilinear stress strain curve. The Finite Element Model is shown in Figure (7.11). The results of this were compared with the rigid body plastic hinge model (Figure 7.12 and 7.13). They are found to be in good agreement.

7.6 Nonlinear Dynamic Analysis

In this analysis, all the bodies were assigned an initial velocity and a step load was applied at node 20 (Figure 7.11). The initial velocities of all the bodies / links were found using classical graphical vector polygon method. The response obtained from rigid body plastic hinge model and from the finite element analysis were found to be in good agreement. Some of the results are shown in Figures (7.14) and (7.15).

7.7 Inclusion of Flexibility with the Plastic Hinges

To improve the accuracy of the rigid body plastic hinge model, flexibility into the members was introduced. The flexible aviation seat model is shown in Figure (7.16). Here, the two legs supporting the seat pan have been modelled as flexible bodies with four bar elements. Each flexible body has 15 degrees of freedom, which after the application of mean axis theorem reduces to 12. Total degrees of freedom of the system is 24. As before, the model has 5 plastic hinges. The analysis was carried out using the general purpose code RIFLEX. All the bodies were subjected to initial velocity and a step load was applied at node 3 on the front leg (Figure 7.16). Table (7.2) gives the details of the rigid flexible model of the aviation seat structure. The acceleration response of the seat pan analyzed with rigid body and flexible body models are shown in Figure (7.17). They have the same tendency. However, due to the inclusion of the flexibility the pan response does not abruptly change.

7.8 References

1. Pereira, M.S., Gim, G., Lankarani, H.M. and Nikravesh, P.E., "Technical Data and a Plastic Hinge Model for M151-A2_Rollerbar Cage," Department of Aerospace and Mechanical Engineering, University of Arizona, Tucson, March 1987.

2. Nikravesh, P.E., "Computer Aided Analysis of Mechanical Systems," Prentice Hall Publications, 1988.

TABLE 7.1- NODAL DISPLACEMENTS OF THE SEAT STRUCTURE

Node Number	Plastic Hinges	Finite Elements
3	0.0054	0.0064
5	0.0109	0.0104
10	0.0106	0.0105
15	0.0105	0.0102
20	0.0052	0.0081

TABLE 7.2 - DATA FOR RIGID FLEXIBLE AVIATION SEAT STRUCTURE

CHARACTERISTIC	VALUE				
Seat structure dimension	Refer Figure 4.15.				
Section of the beam	Hollow Circuar Section 1.75" OD & 0.083" Thick				
Material of the beam	Al 2024-T4 ; E=72e9 N/m^2; Den=2780 Kg/m^3				
Initial Velocitites (m/sec)	Bodies	Body 2	Body 3	Body 4	Body 5
	X Velocity	6.144	12.144	6.0	0.0
	Y Velocity	-1.025	-1.025	0.0	0.0
	Angular Velocity	-40.322	5.383	-33.488	0.0
Type of load	Step load of -15000N @ node of 3 of Flexible body4				

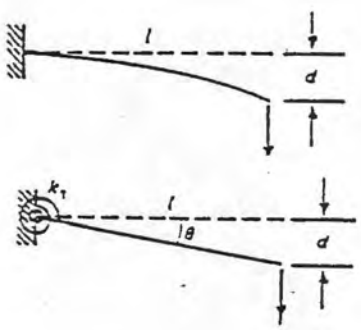

FIGURE 7.1 PLASTIC HINGE MODEL OF A CANTILEVER BEAM

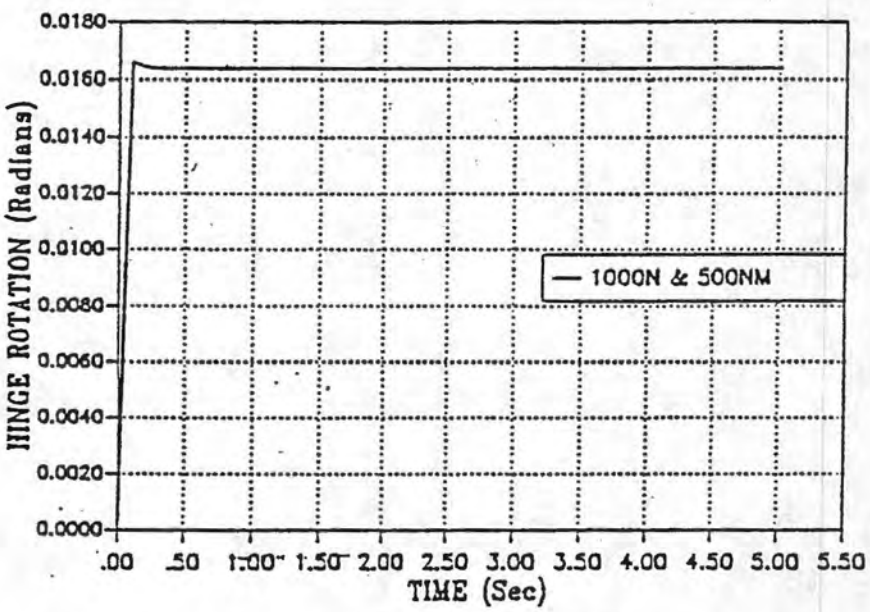

FIGURE 7.2 HINGE ROTATION OF A CANTILEVER BEAM

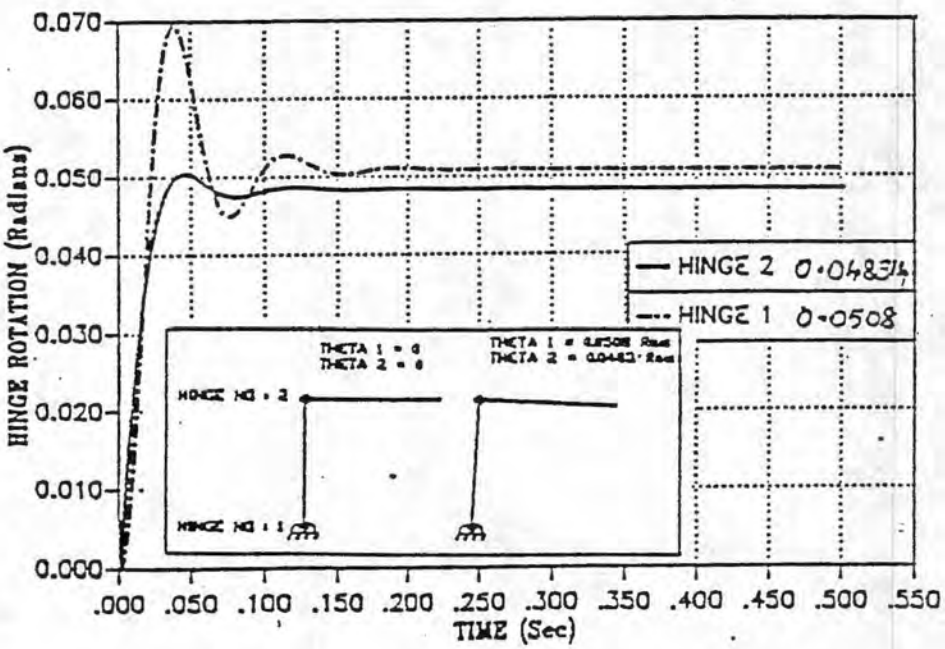

FIGURE 7.3 HINGE ROTATIONS OF L-FRAME

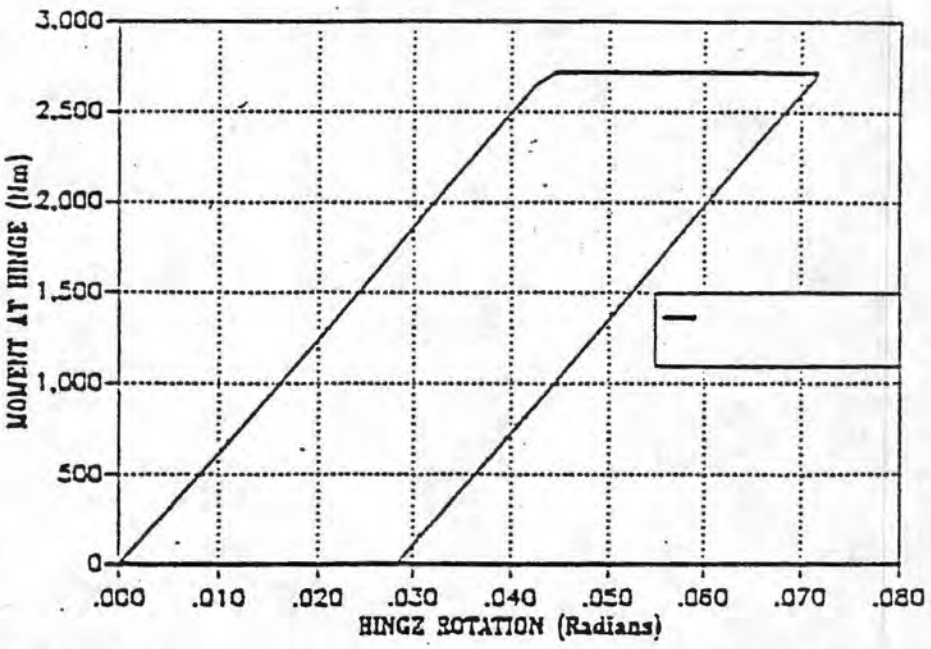

FIGURE 7.4 MOMENT-ANGLE DIAGRAM FOR A CANTILEVER BEAM LOADED AT THE TIP

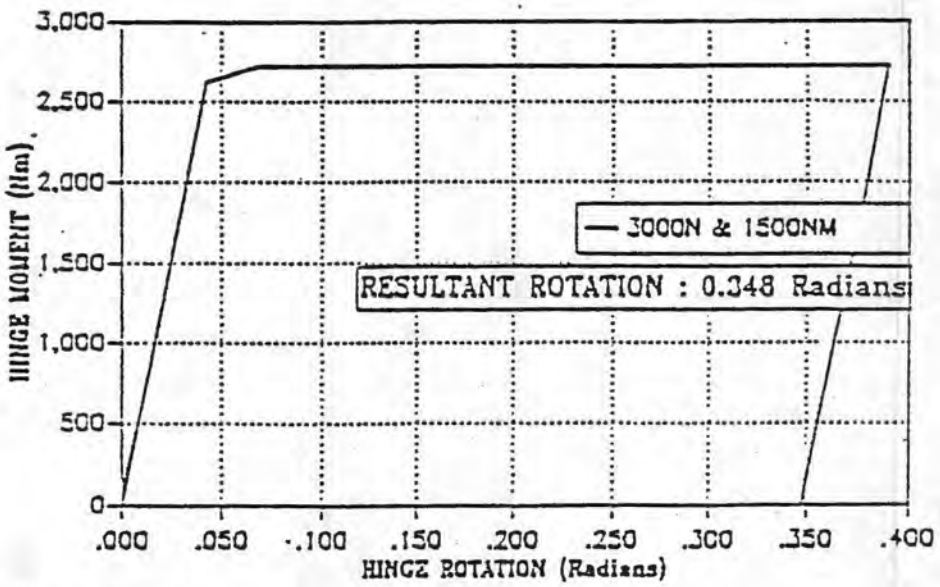

FIGURE 7.5 MOMENT-ANGLE DIAGRAM FOR AN L-FRAME (HINGE 1)

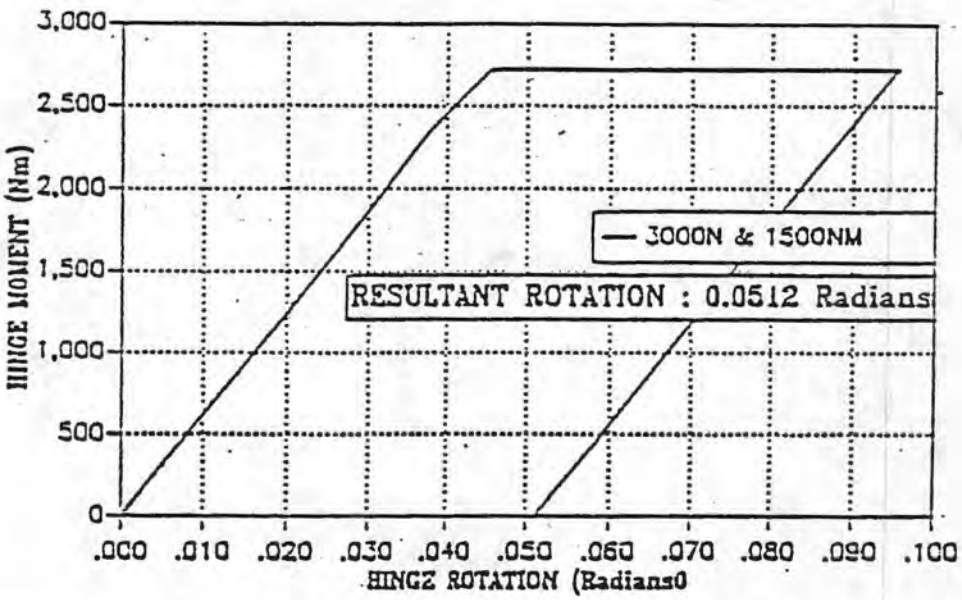

FIGURE 7.6 MOMENT-ANGLE DIAGRAM FOR AN L-FRAME (HINGE 2)

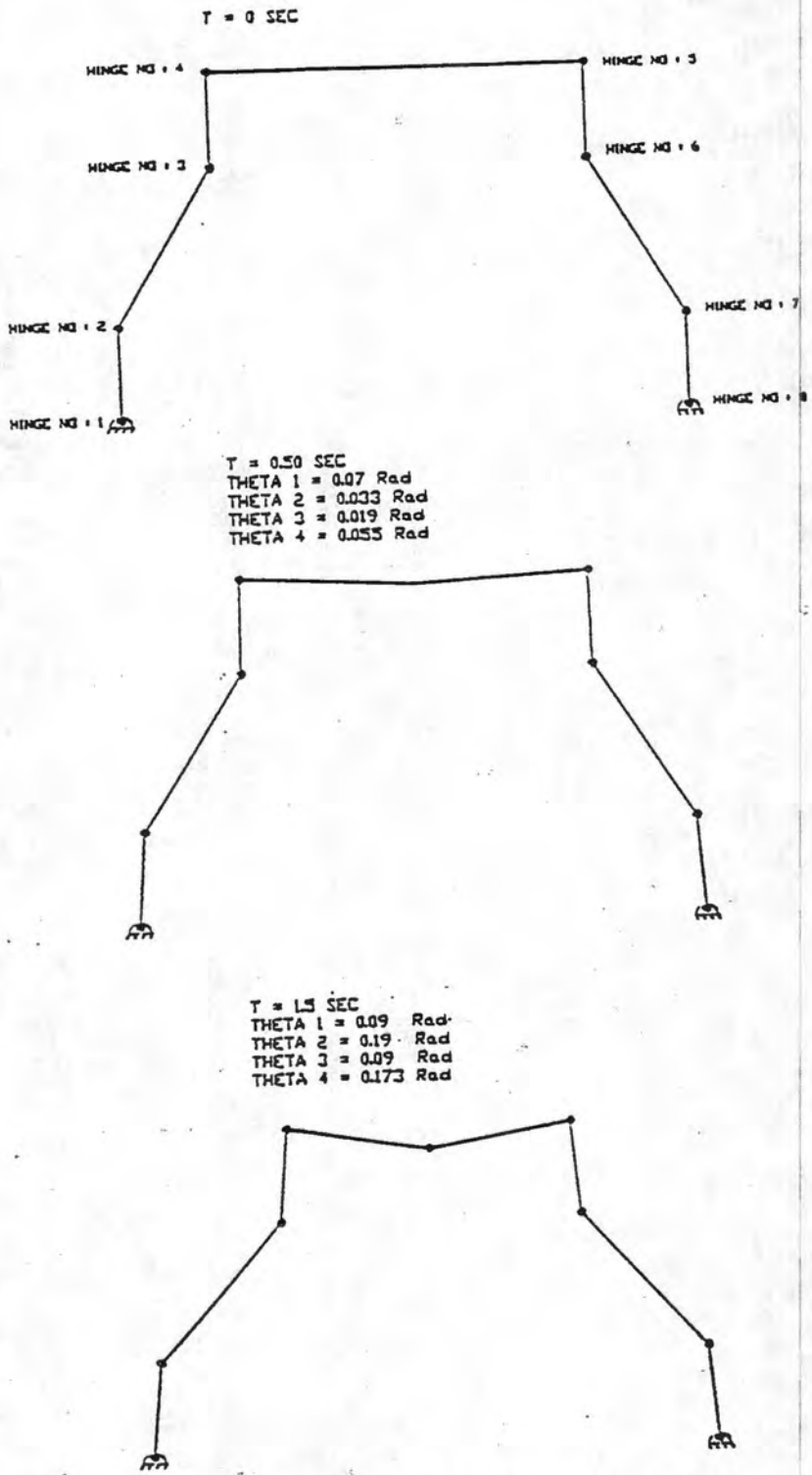

FIGURE 7.7 RESPONSE OF A TORQUE BOX USING THE PLASTIC HINGE MODELING

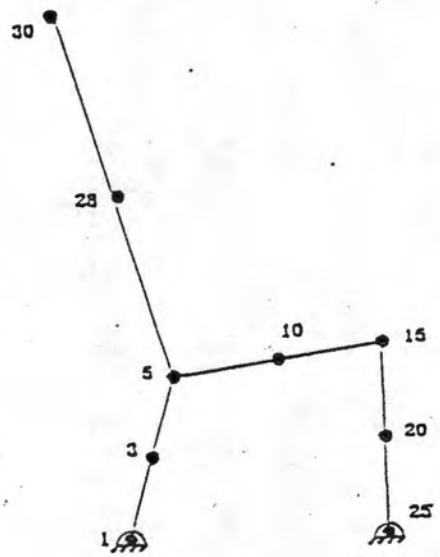

FIGURE 7.8 PLASTIC HINGE MODEL OF AN AVIATION SEAT

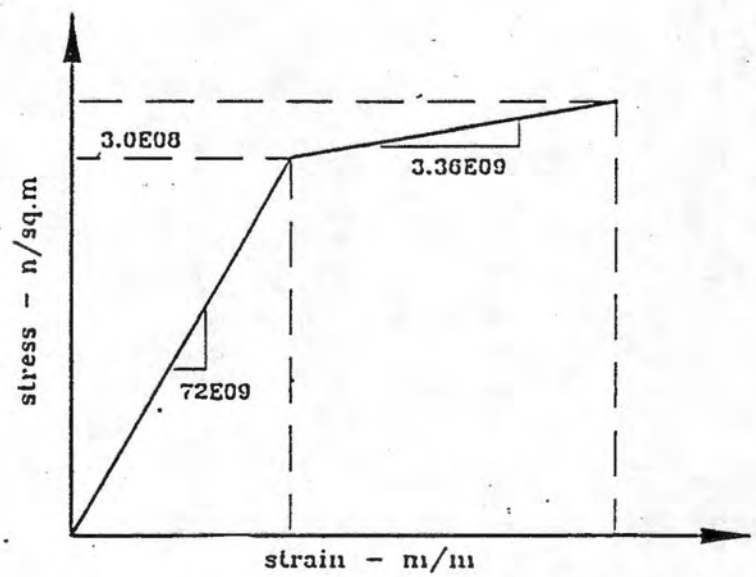

FIGURE 7.9 STRESS STRAIN RELATIONSHIP FOR AVIATION SEAT MODEL

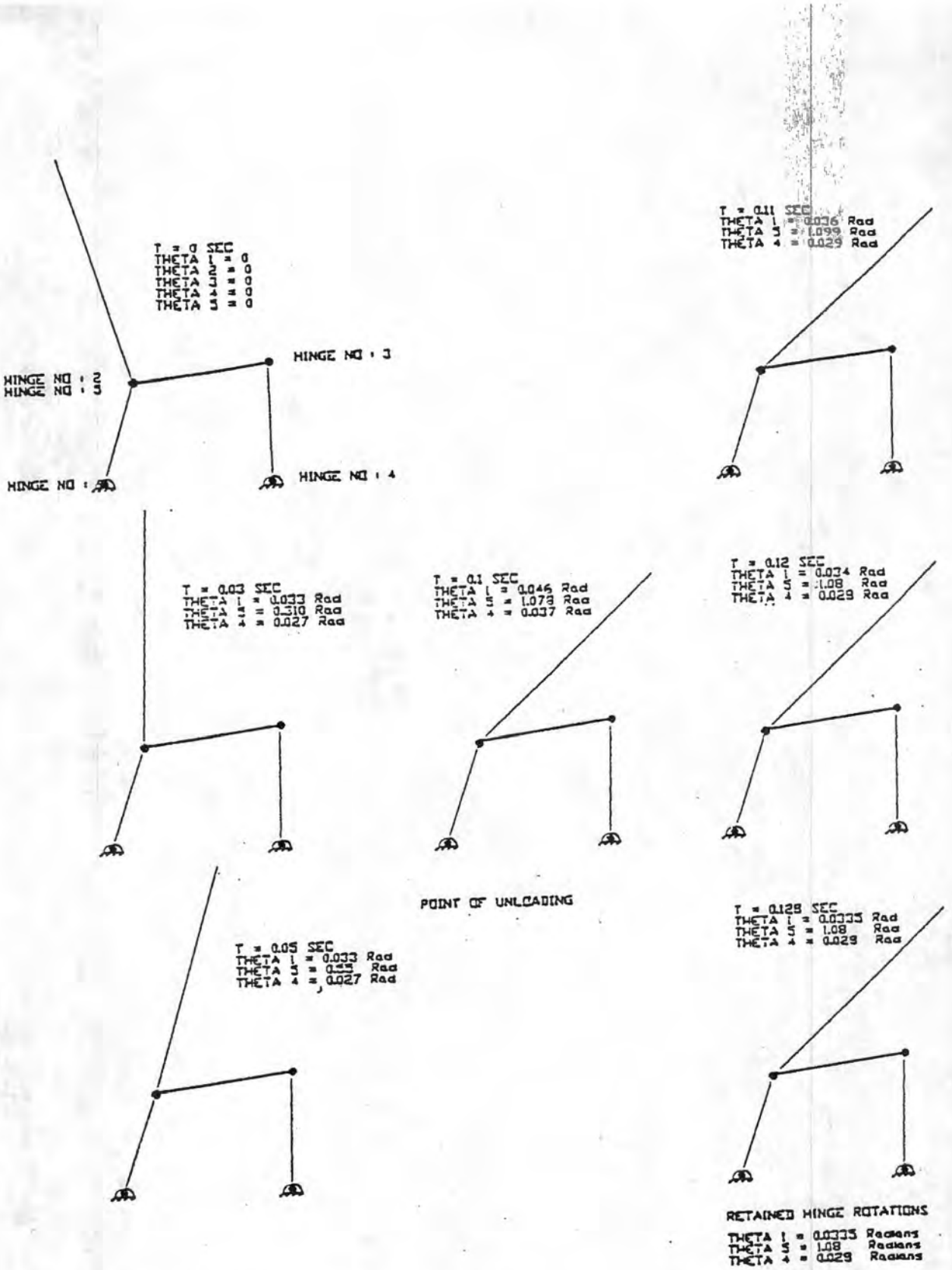

FIGURE 7.10 RESPONSE OF AN AVIATION SEAT USING PLASTIC HINGE MODEL

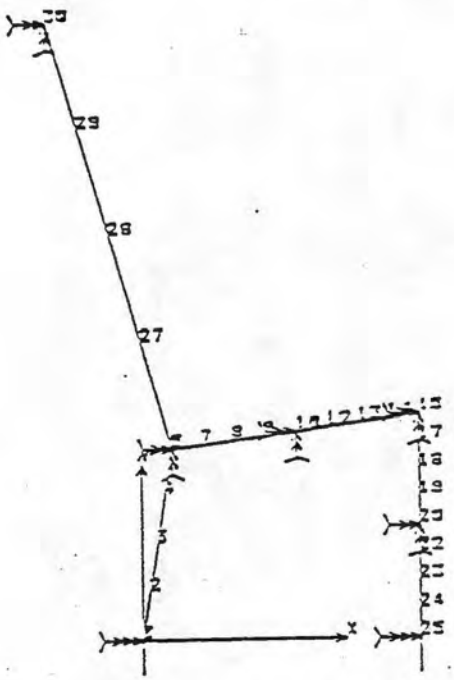

FIGURE 7.11 FINITE ELEMENT MODEL OF AVIATION SEAT

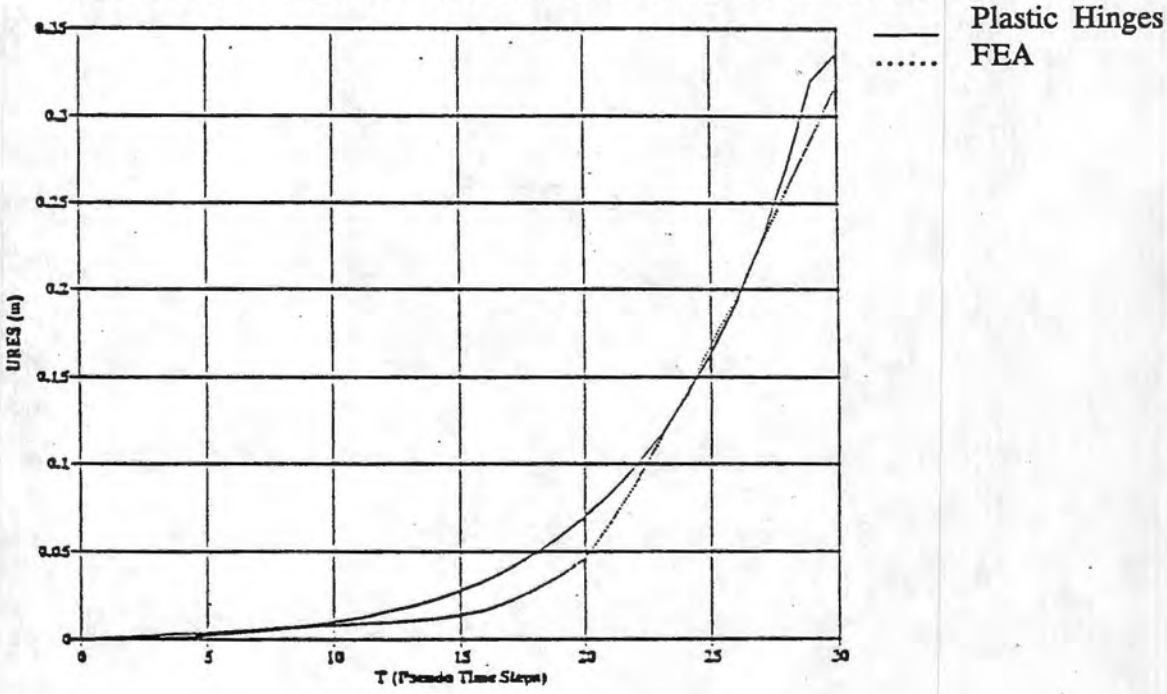

FIGURE 7.12 DISPLACEMENT AT NODE 3

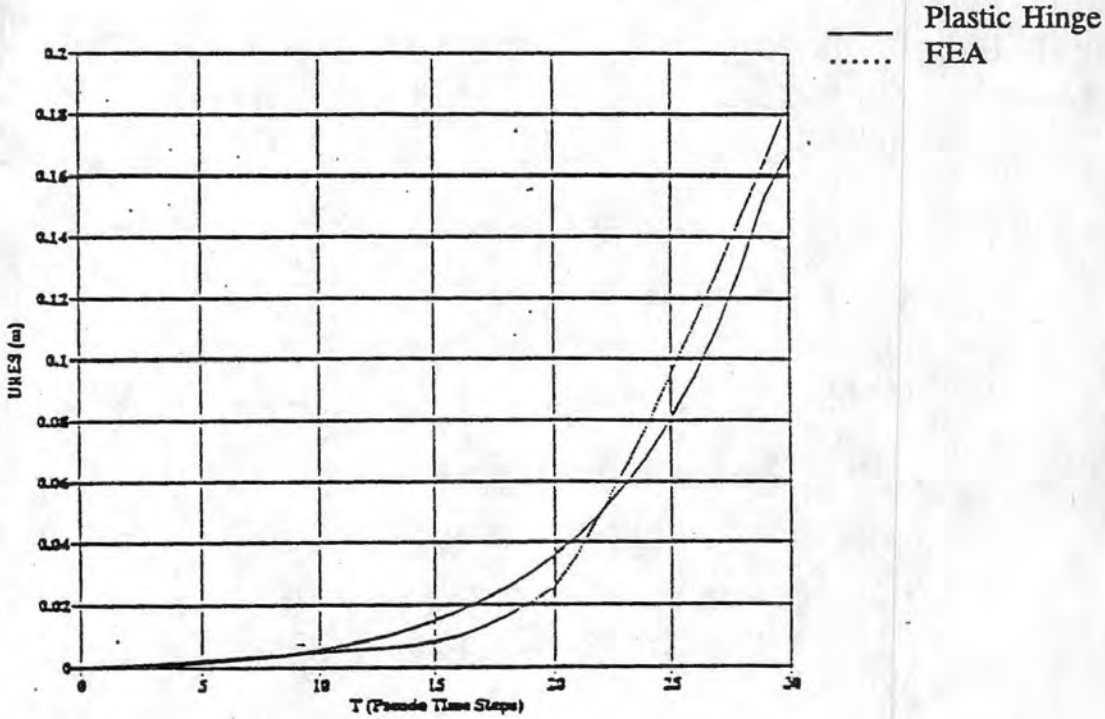

FIGURE 7.13 DISPLACEMENT AT NODE 5

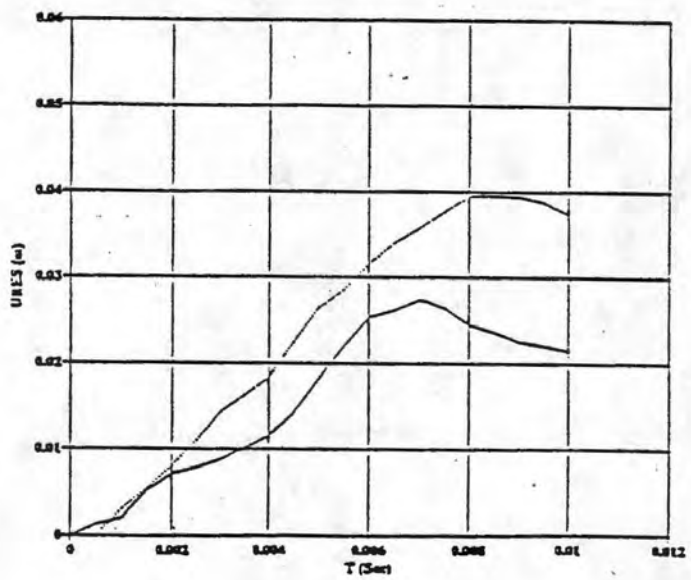

FIGURE 7.14 DISPLACEMENT AT NODE 3

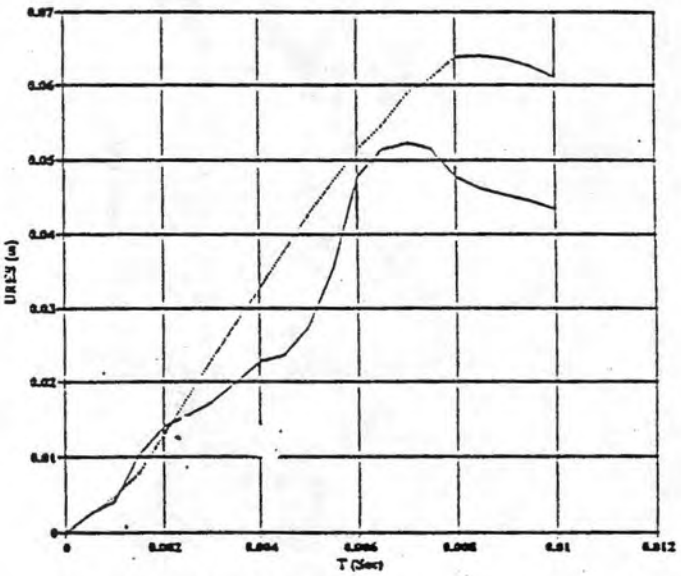

FIGURE 7.15 DISPLACEMENT AT NODE 5

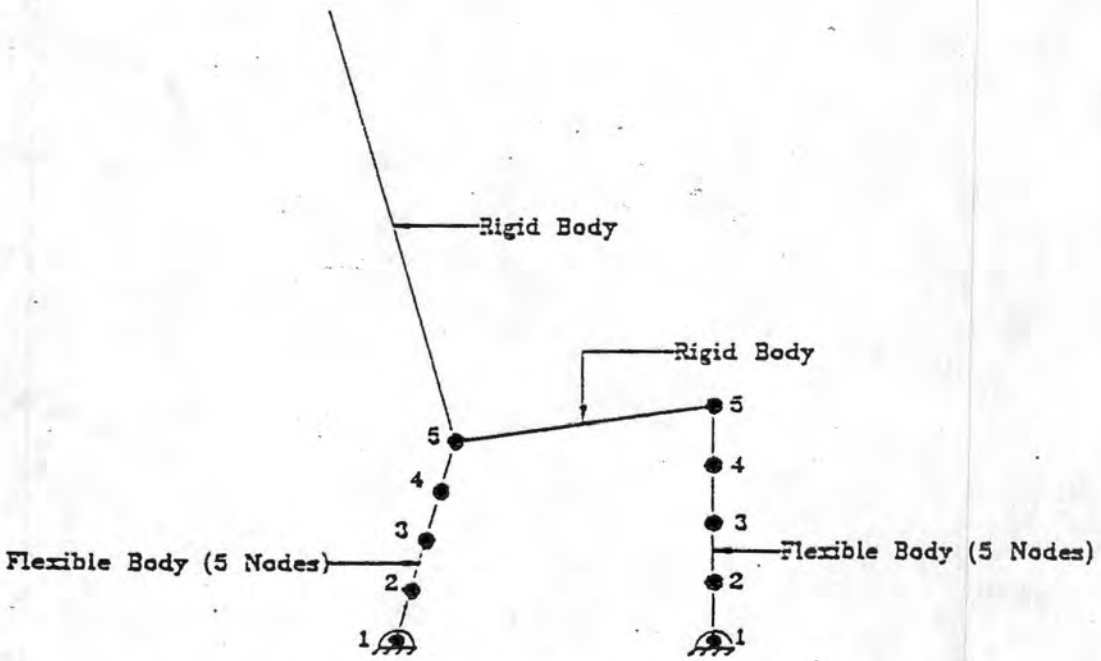

FIGURE 7.16 RIGID FLEXIBLE AVIATION SEAT MODEL

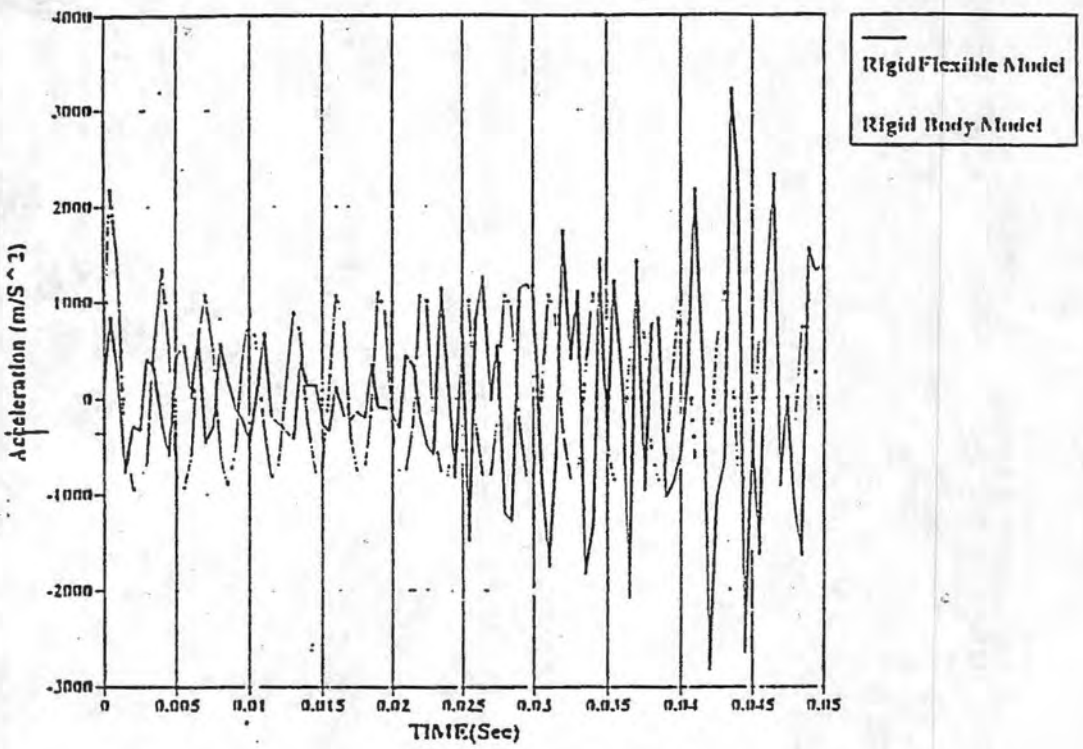

FIGURE 7.17 ACCELERATION RESPONSE OF THE SEAT PAN

8. CONCLUSIONS AND RECOMMENDATIONS

8.1 Conclusions

The knowledge of occupant responses in a crash environment helps in understanding and determining the type and probable causes of injuries that may be sustained by pilot or passengers during a crash. The results from the investigation may be used in the design of safer restraints system and occupant surroundings. Simulation of the occupant responses using the concept of multibody dynamics and finite element approaches on the computers is an efficient way of gaining insight of the occupant motion in the preliminary design. The following lists the conclusions from the tasks conducted in this investigation.

1. Dynamic tests were conducted as per FAR Part 23.563.b(1) & b(2) at different deceleration loads of 15, 19, 25 and 32 g's with hybrid II ATD on an iron seat and restrained by a two point system.

2. A comparative study of codes SOMLA/TA, MADYMO, ATB was made. The results from these codes were compared with the test results, tests being conducted in various configurations. It was found that the codes predicted the maximum head acceleration reasonably accurate. However, the HIC and lumbar load values were not accurate all the time. The differences can be attributed to difficulties and inaccuracies in modelling the human body.

3. For better prediction of the lumbar loads from the analysis tools, a nonlinear finite element model of the lumbar spine was developed and included in the multibody model of the occupant in the code SOM-LA/TA using a kineto-static methodology.

4. The improved code SOM-LA/TA was used to duplicate the dynamic tests conducted. The code has shown much improvement in the prediction of both the peak and the trend of the lumbar load than the original code.

5. In an effort to obtain the response of occupants other than 50 th percentile male, data were collected for a 3 year old child (both dummy and human), and necessary input files were generated for SOM-LA/TA. Injury criteria for child: HIC, lumbar load and femur load were scaled down for the 3 year-old child.

6. An integrated child seat has been designed using MADYMO. The effect of using different seat cushions on the value of HIC and Lumbar load has been studied. The developed seat has been simulated in frontal, oblique and vertical impact environment.

7. A methodology for the analysis of aircraft seat structures using rigid multibody motion coupled with plastic hinge theory has been developed. This technique is computationally efficient and less time consuming. It is seen to predict results very close to Finite element analysis results. Also, flexibility to the structure has been added to improve the

performance of the analysis. This technique serves as a powerful tool to the design engineer for preliminary design analysis.

8. Head injury due to impact of head onto bulkheads, hard surfaces etc. were studied using Finite element analysis technique. Use of proper padding material on the potential target areas was found to be effective in reducing head injury. Results from head impact analysis onto different padding materials being analyzed through finite element analysis, were found to very close to the experimental results. A HIC response surface based on design of experiments techniques for different values young's modulus, ultimate strength was developed. From this the HIC value can be predicted for a given value of young's modulus and ultimate strength.

9. Design and fabrication of nonsled test setup has been discussed. The pendulum type designed is economical and easy to operate compared to the conventional sled test setups. Using this setup, the sled tests can be duplicated. The pendulum setup is installed in the impact dynamics lab at NIAR. Padding tests were conducted on the setup to evaluate the HIC.

8.2 Future work

1. Examine the responses of occupants on side-facing seats:
   Three dimensional modelling of the occupants; side impact dummy testing - SID, BIOSID, EUROSID; and component testing.

2. Identify factors and quantify their effects on HIC.
   Type of ATD, initial position, restraint system, seat structures, seat cushion, seat pitch, deceleration pulse and compliance properties and boundary conditions of panels (in case of a head impact).

3. Correlation between the full-scale sled tests and head component tests.
   Component testing is much more repeatable; it is more controllable; the elapsed time for evaluation the designs, materials and other significant parameters is reduced. However, it must be shown how well the component tests represent the full-scale tests.

4. Use the head strike tests for acquiring information on methods for reducing HIC: material size, boundary conditions and thickness.

5. For different materials, find the required crush depth as a function of impact velocity for a HIC < 1000. Develop a database of the head component test results.

6. Develop analytical capabilities for reproducing the "Bowling Ball" drop tests conducted at CAMI. Use a nonlinear finite element model of the ATD head and padding material on the panel using the sub-structuring technique. Utilize the codes COSMOS and

DYNA3D.

7. Expand the database of occupants from the 50 th percentile male and 3 -year old child to other sizes. Quantify the effect of occupant size on the response of a seat/occupant/restraint system. Develop injury criteria for a range of occupant sizes and ages.

8. Enhance the graphical animation program to provide a quick re-construction of the analysis of the experiment.

9. Examine the possibility of using a neck injury criterion. Develop detailed modelling of the cervical paine; examine the limits on neck moments and corridors for neck injuries.

10. Examine the proposed Part 23.563.b(1) & b(2) and other conditions for the commuter aircraft and recommend a suitable test program.

11. Develop guidelines on design and development of both add-on and integrated child seats and restraint systems.